SANDIA REPORT
SAND2022-12745
Printed September 2022

Sandia National Laboratories

Extension of Interferometric Synthetic Aperture Radar to Multiple Phase-Centers: Midyear LDRD Final Report – second edition

Douglas L. Bickel and John M. DeLaurentis

Prepared by
Sandia National Laboratories
Albuquerque, New Mexico
87185 and Livermore,
California 94550

Issued by Sandia National Laboratories, operated for the United States Department of Energy by National Technology & Engineering Solutions of Sandia, LLC.

Available to DOE and DOE contractors from
U.S. Department of Energy
Office of Scientific and Technical Information
P.O. Box 62
Oak Ridge, TN 37831

Telephone: (865) 576-8401
Facsimile: (865) 576-5728
E-Mail: reports@osti.gov
Online ordering: http://www.osti.gov/scitech

Available to the public from
U.S. Department of Commerce
National Technical Information Service
5301 Shawnee Rd
Alexandria, VA 22312

Telephone: (800) 553-6847
Facsimile: (703) 605-6900
E-Mail: orders@ntis.gov
Online order: https://classic.ntis.gov/help/order-methods/

Extension of Interferometric Synthetic Aperture Radar to Multiple Phase-Centers: Midyear LDRD Final Report – second edition

Douglas L Bickel and John M. DeLaurentis

Abstract

This document contains the final report for the midyear LDRD titled “Extension of Interferometric Synthetic Aperture Radar to Multiple Phase-Centers.” This report presents an overview of several methods for approaching the two-target in layover problem that exists in interferometric synthetic aperture radar systems. Simulation results for one of the methods are presented. In addition, a new direct approach is introduced.

Acknowledgements

This document is a final report for a Sandia National Laboratories FY2005 Mid-year Laboratory Directed Research and Development (LDRD) project.

Its reissue as a second edition is the result of an unfunded Research and Development effort.

Contents

List of Figures

Acronyms and Definitions

1-D, 2-D, 3-D	1-, 2-, 3-Dimensional
AP	Alternating Projection
ATR	Automatic Target Recognition
CLEAN	[image enhancement technique]
GMTI	Ground Moving Target Indicator [Radar]
JSTARS	Joint Surveillance and Target Attack Radar System
IFSAR	Interferometric Synthetic Aperture Radar
LDRD	Laboratory Directed Research and Development
LIDAR	Light Detection and Ranging
ML	Maximum Likelihood
MUSIC	[image enhancement technique]
PDF	Probability density Function
PHD	Pisarenko Harmonic Decomposition
RELAX	[image enhancement technique]
RTV	Rapid Terrain Visualization
SAR	Synthetic Aperture Radar
SNR	Signal to Noise Ratio
STAP	Space Time Adaptive Processing

Foreword

This report is a second edition of a previous report of otherwise the same name. The earlier report issued in 2005 and was restricted with a limited distribution. This report has undergone a review to lift the distribution restrictions, and now is unrestricted. Some minor editing and slight reformatting ensued, otherwise it is the same content.

Classification

The specific mathematics and algorithms presented herein do not bear any release restrictions or distribution limitations.

This report formalizes preexisting informal notes and other documentation on the subject matter herein.

This report has been approved as Unclassified – Unlimited Release.

OBJECTIVE

This report is to serve as the final report for the "Extension of Interferometric Synthetic Aperture Radar to Multiple Phase-Centers" midyear LDRD. The objective of the LDRD is stated in the following abstract submitted as part of the LDRD process:

> *Interferometric Synthetic Aperture Radar (IFSAR) is a technology which has the potential to satisfy the high demand for accurate and timely terrain data from both government and commercial entities. IFSAR will also likely be used in targeting systems in the near future. Currently, Sandia is a recognized leader in IFSAR systems and technologies. The next major advance in IFSAR will be in the area of multiple phase-centers.*
>
> *Sandia's Rapid Terrain Visualization IFSAR system has already shown that multiple phase-centers provided a significant advance in phase unwrapping. In addition, multiple phase-centers could provide improvements in resolution. More importantly, multiple phase-center IFSAR processing takes a large step in the direction of true 3-D imaging, which allows resolution of multiple targets in layover regions. The solution to this problem is important for urban scenes, targeting, imaging in foliage, and automatic target recognition (ATR). Results from this project will remove one of the competitive advantages that LIDAR has over IFSAR in urban environments.*
>
> *In addition, results from this work would have significant spill-over into other key technology areas, such as multiple platform bistatic imaging, and endo-clutter ground moving target indication (GMTI). The multiple phase-center IFSAR work is highly related to the problem of position location of moving targets, and it is likely that results from this work could be re-used in this problem.*

SCOPE OF WORK

The scope of work, as presented in the original LDRD, is given below. At the time the LDRD was written, it was hoped that the LDRD would find support to become a full LDRD rather than just a midyear LDRD. The additional work of a full LDRD would allow us to collect, calibrate and process real data sets using the algorithms presented in this document. An LDRD extension would have enabled work on enhancing these algorithms and practical implementation in terms of efficiency of the algorithms presented in this document.

> *For the remainder of FY05, the work would be focused on the development of algorithms and techniques for processing multiple phase-center IFSAR data. Specifically, work would be performed to develop algorithms for 3-D target resolution in layover for 3 to 4 phase-centers. The work would involve analysis and simulation. If there are additional funds available at the end of this project, an attempt will be made to apply the techniques to actual SAR data sets. This assumes that available data sets are adequate for this LDRD.*

INTRODUCTION

The next generation of radar systems will support multiple phase-centers (more than two) for introducing more sophisticated radar applications. An example of such a system is the JSTARS radar system used to track moving targets. With the success of the JSTARS radar system, other multiphase center radars, such as the German AER-II [1], will become more prevalent.

Sandia National Laboratories has been a recognized leader in advanced systems, algorithms, and technologies. To maintain this leadership, SNL needs to become a leader in the next generation of radars.

As mentioned, multiple phase-center systems are important for ground-moving-target-indicator (GMTI) radar systems. SNL has also developed a 3-phase center system for mitigating ambiguities in the Rapid Terrain Visualization (RTV) terrain mapping radar [2].

The focus of this report will be on the application of multiple-phase-center system to resolving the radar layover problem. This problem is a step in the direction of true 3-D imaging with a radar system.

OVERVIEW

The document is organized to give a description of the problem and examine proposed solutions. In particular, we focus on the two-target layover problem in detail. We show the similarities and differences of this problem with the endoclutter ground moving target problem. We show that the endoclutter ground moving target problem is a subset of the two-target layover problem.

The document then examines solutions to the problem. Many of the solutions proposed in literature are not well-suited for the two-target layover problem. One particular solution proposed in literature that has some promise, is examined. This is the spectral MUSIC algorithm. Using simulation, we show some of the limitations of this approach.

Finally, we present a new direct approach that focuses specifically on the two-target problem. The solutions presented in literature tend to attempt to solve the general number of targets problem.

THE TWO-TARGET LAYOVER PROBLEM

Since this is a mid-year LDRD and funding is limited, this document will focus on the resolution of two targets in layover under the assumption that the volume available for the antennas is limited. It turns out that a very important layover case is the two-target case of layover of a building [3, 4, 5]. Even in the more complicated case of vegetation and steep mountains, we should be able to derive more information about the target structure using 3 antennas than we could with 2 antennas. Therefore, the two-target case is a very important problem to solve. Also, the limited volume case is generally very important because space and separation of antennas is often limited unless multiple passes of the sensor are used. Multiple passes of the sensor bring their own set of issues, such as temporal decorrelation and flight path estimation and resampling [6] Nevertheless, the multiple pass problem is an important problem, but not one we will dwell on in this report.

In traditional two-phase-center interferometric SAR (IFSAR), there is an assumption that each range-Doppler cell contains only a single target or spatial frequency. Layover causes this assumption to be violated. Note that a finite resolution cell width in terrain also causes this assumption to be violated. We only consider this latter issue very briefly in the wideband case where we have a "large" spread of spatial frequencies within the range-Doppler resolution cell. In particular, in this report will focus on two distinct spatial frequencies within a single range-Doppler resolution cell. As stated above, we will refer to this as the two-target layover problem, which we now describe below.

The case of two targets in layover for the standard two-phase-center IFSAR system was presented in [7]. Another perspective of this issue, related to the GMTI problem, was presented in [8]. The bottom line is that there are not an adequate number of degrees-of-freedom to resolve two targets with only two phase centers. We need at least 3 or more phase centers to resolve the two-target case. As mentioned above, a very important layover case is the two-target case of layover of a building. The problems caused by two-antenna IFSAR processing of a building layover is shown in the Figure 1. It is common to see an additional edge in IFSAR on the side of the buildings nearest the radar, as highlighted by the red arrows in the Figure. This additional edge has been termed the "front porch" effect [4] because it was first noticed in high-resolution IFSAR data from an SNL radar and appeared as a false porch or deck on the near-range side of one of the buildings within the Tech Area.

Figure 2 illustrates the geometry of building layover in a cartoon. The figure shows that the radar sees the response from the top of the building and the ground within the same range-Doppler resolution cell. The effect of using two phase centers to examine the two targets, is that we can only estimate one direction-of-arrival for both targets. Depending upon several issues, which will be discussed shortly, the result of the layover is potentially lower correlation (increased position "noise"), and a displaced target location. On the average, the two-phase-center IFSAR system will report a target location at an angle between the top of the building and the ground. The target is measured by the radar to be within the range bin illustrated, and so the final solution must be located somewhere along the range bin circle. Thus, the front of the building in traditional IFSAR systems appears to be lower and pulled out, creating an artificial porch.

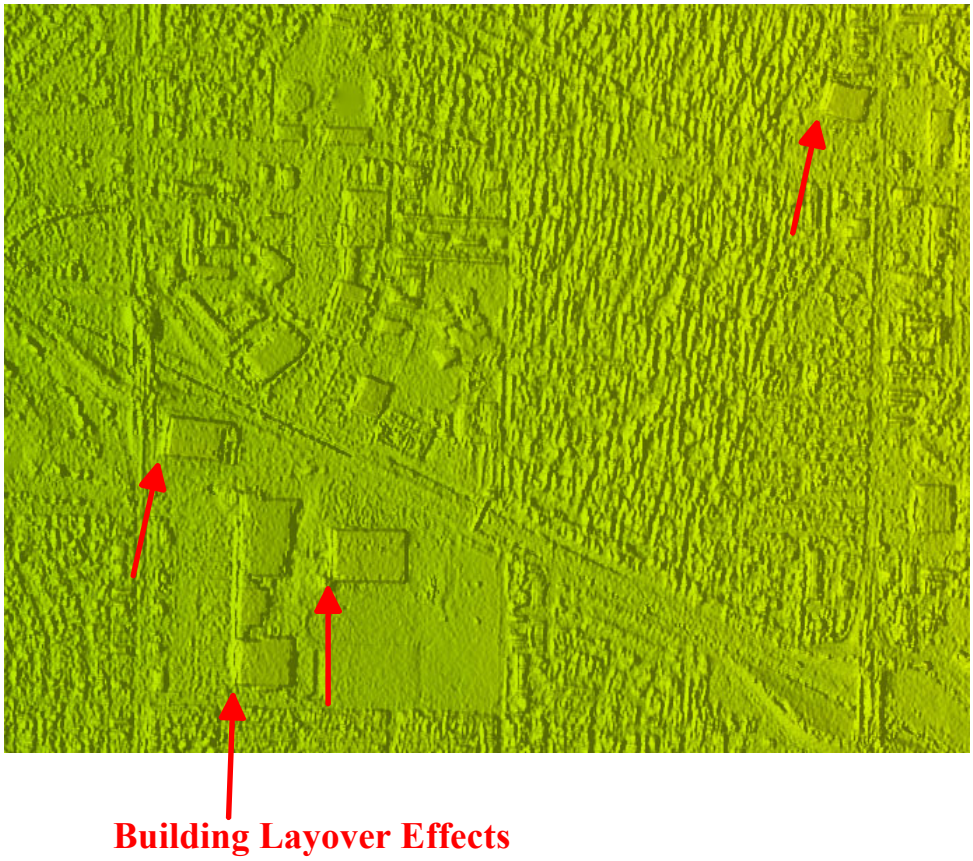

Figure 1. Examples of Building Layover in Shaded Relief DEM Data from RTV Albuquerque Collect.

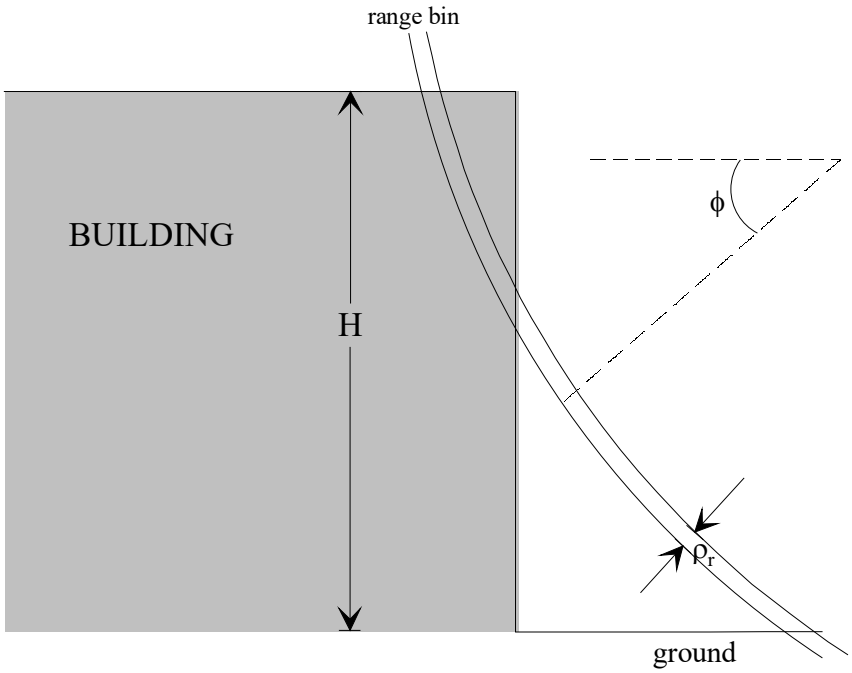

Figure 2. Illustration of Building Layover

The mathematical description of building layover was first discussed in [7]. Following this reference, the van-Cittert Zernike theorem shows that for layover the complex correlation due to layover, μ, is given by:

$$\mu = \frac{\sin(\pi X)}{\pi X}\left\{\beta \exp\left[j\alpha\left(\frac{H}{2}\right)\right] + (1-\beta)\exp\left[j\alpha\left(-\frac{H}{2}\right)\right]\right\} \tag{1}$$

where

$$X = \frac{2B\rho_r \tan\phi}{r_0\lambda}$$

$$\beta = \frac{I_{roof}}{I_{roof} + I_{ground}}$$

$$\alpha = \frac{4\pi B}{\lambda r_0 \cos\phi}$$

B = the orthogonal component of the baseline

I_{roof}, I_{ground} = intensity of return from roof and ground respectively

λ = the wavelength of the radar

r_0 = the range to the target

ρ_r, ϕ, H as shown in Figure 2

The above equation makes the simplifying assumption that the boresight of the antenna is pointed at the center of the building, and that the radar impulse response function is flat across the resolution cell.

Under the condition that the intensity of the roof and the ground are the same in Eq. (1), the last term in this equation becomes a cosinusoidal function of height. Note that in this case, the complex correlation has no phase. This means that the IFSAR will yield a corresponding height of mid-way between the roof and ground. This is the "front-porch" height. In addition, this cosinusoidal function modulates the correlation as a function of the height of the building relative to the wrap height of the IFSAR sensor. This latter fact is interesting. It says that two antennas do yield two pieces of information. The phase of the complex correlation yields an estimate of the intensity weighted positions within the resolution cell. This is not news for IFSAR. The other is the modulus (magnitude) of the correlation, which yields information about whether or not the assumption of one target is valid. This fact will be discussed more in the model order section of this document.

In general, Figure 3 illustrates the two-target problem that we address in this document.

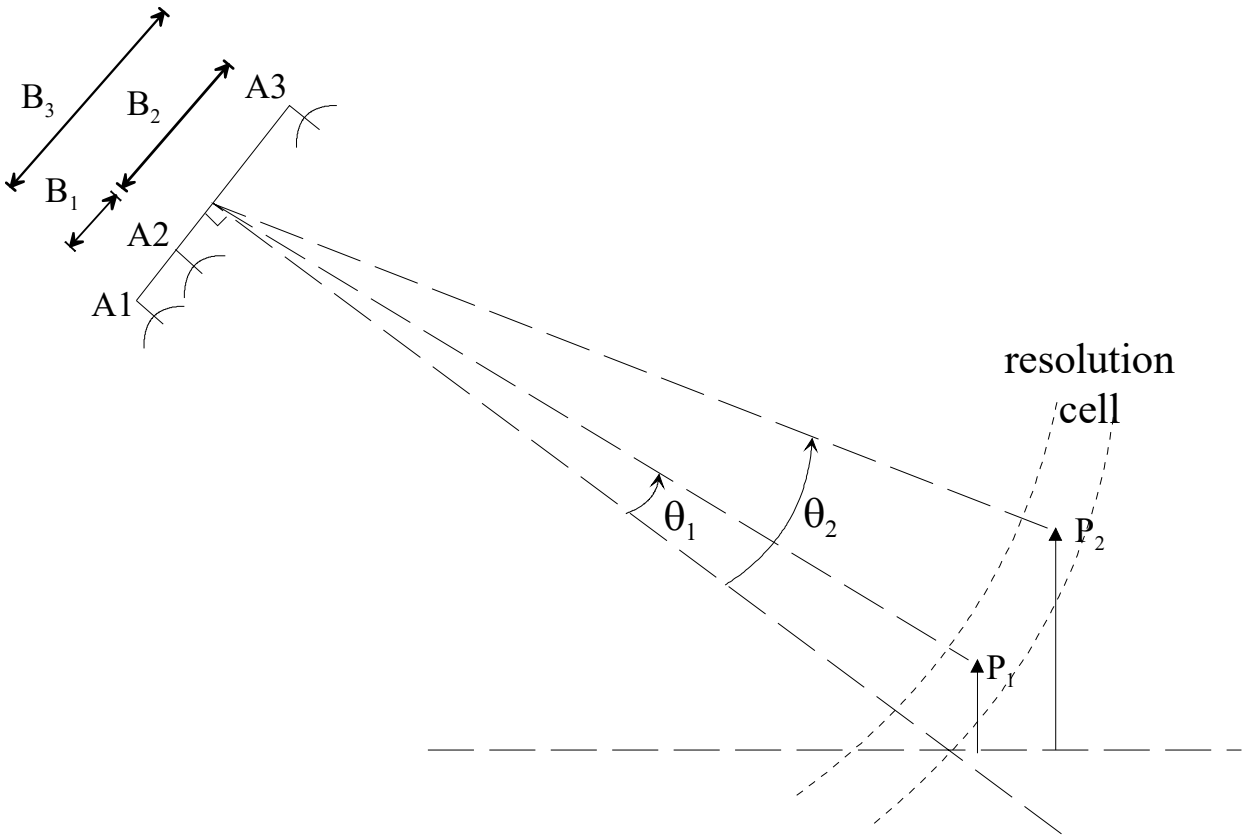

Figure 3. Illustration of Geometry for Two-Target Problem

RELATIONSHIP OF THE LAYOVER PROBLEM TO ENDOCLUTTER GMTI

A very important problem in multiple phase centers is the location of a moving target within the main beamwidth of the antenna. Note that the detection of a moving target within the main beam of the antenna is a different problem than the location of a moving target within the main beam of the antenna. In general, deciding whether a target is moving or not takes less information than saying how fast the target is moving. The result is that the location of a moving target requires more degrees-of-freedom, hence more phase-centers, than the moving target detection. We will focus on the moving target location and its relationship to the layover problem, so the title of this section is a little misleading.

The presentation and conclusions in this section are somewhat simplified from the full-blown space-time-adaptive-processor (STAP) development to facilitate the understanding of the relationships of these problems. The general conclusion that will be presented is valid. The conclusion is that the layover problem is the more general case and requires more sophistication in the processing than does the moving target location problem. Note that this does not mean that the resolution of one problem versus the other is easier to accomplish. It only means that the moving target location is a subset of the general layover problem and due to its nature, permits simpler algorithms to resolve.

Assume that we have a moving target that has a location within the main antenna beam. The instantaneous Doppler of this moving target in a SAR image will be the combination of the Doppler due to the moving target and due to the moving SAR platform. This moving target will "layover" onto a range-Doppler resolution cell that has the same Doppler due to the motion of the SAR platform. In other words, the moving target will "layover" onto a stationary clutter cell. Now if the amplitude of the moving target is much brighter than that of the clutter that it "lays over" onto, we could use a simple along-track interferometer or monopulse to estimate the true location of the moving target. Then, given the estimate of the location of the target, we could remove the component of Doppler due to the moving SAR platform from the total Doppler and resolve the radial velocity from the residual Doppler. Note that the assumption that the moving target is much brighter than the clutter in the same range-Doppler cell is a crucial assumption. This assumption has reduced the required degrees-of-freedom by essentially saying that there is only one target present in each range-Doppler cell. In other words, we are assuming that there is no clutter to interfere with the moving target. The result is that a standard two-phase-center antenna used as an interferometer is sufficient to resolve this problem. We note that this is like the standard IFSAR problem where we can assume a single spatial frequency within each range-Doppler resolution cell as observed by the aperture along the baseline. The only difference is that we orient the baseline in the along-track direction for GMTI, and in the elevation direction for IFSAR.

The problem becomes more complicated when we cannot ignore the contribution of the clutter that shares the same range and Doppler resolution cell with the moving target. We established one of the bounding cases above when we assumed that the clutter had essentially zero power. This leads to the two-phase-center interferometer detecting the true location of the moving target. The other bounding case is where the moving target returns essentially zero power, in which case

we will estimate the location of the stationary clutter cell with the two-phase-center interferometer. It should be noted that in this latter case, the clutter location should be the same as we would estimate from Doppler. (As a hint of things to come, this last note will turn out to be the key to the discussion in this section.)

Now we discuss what happens between the two bounding cases. To do this, we will simplify the discussion by presenting only the probabilistic expected result, which allows us to avoid the difficulties of fluctuation statistics, etc. On the average, the target location estimated by a two-phase-center antenna, where neither the moving target nor the clutter is negligible, will be somewhere between the true location of the moving target and the location of the clutter. The average estimated location will be weighted by the relative intensity of the two targets. In other words, it will follow a similar development to the building layover presented in a previous section. The estimated location of the moving target by the two-phase-center interferometer will be biased by towards the location of the clutter. The degree of bias will depend upon the ratio of the intensity of the clutter to the intensity of the moving target. Since both intensities are unknown a priori, the best we can do in general is to detect that a mover is present by noting when the location reported by the along-track interferometer differs from the location of the stationary clutter (derived from Doppler) by some specified threshold.

To resolve this problem, we need more information which can be derived from adding a third phase center. We will present this three-phase-center GMTI problem from two different points of view. The first point of view is a very simple one. The second is a little more complicated, but lends itself better to comparison with the elevation IFSAR layover problem. A little thought should convince the reader that the two points of view are essentially equivalent, assuming that baseline decorrelation is negligible.

In the simpler case, we delay each of the phase centers and subtract the results as show in Figure 4. Stationary targets will cancel; whereas, moving targets will not cancel as long as the target is not at a “blind velocity”. With three phase centers, we get two different phase values for the mover delayed in time. We can use this phase difference over time to estimate a Doppler due to target motion. After estimating the Doppler due to target motion, the target location can be separated out from the total Doppler position of the moving target.

Another way to examine the problem, shown in Figure 5, is to look at it as a two-delayed interferometer, instead of as three delayed antennas. To simplify the discussion, we assume that the antennas are equally spaced and travel at a constant velocity. Using these assumptions, we can cancel stationary clutter for antennas and using the resulting pairs after the difference to form an interferometer. In this case, we can estimate the location of the moving target. Using the total Doppler and the estimated location, the line-of-sight velocity of the mover can be estimated.

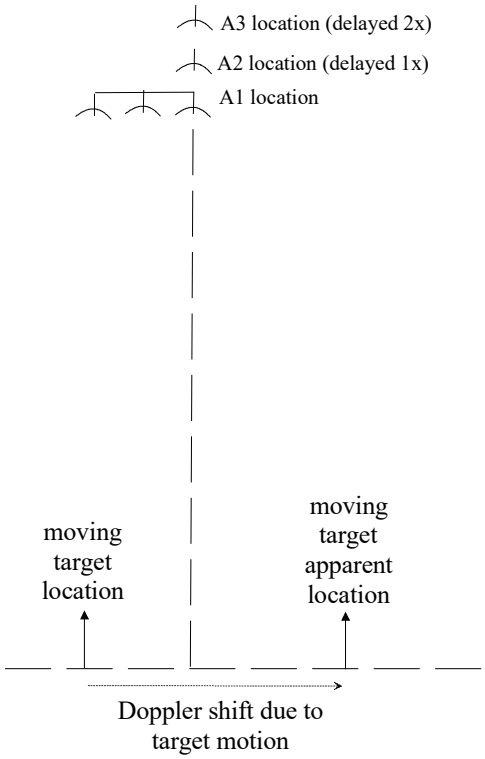

Figure 4. Three Phase-Center Delayed Canceller

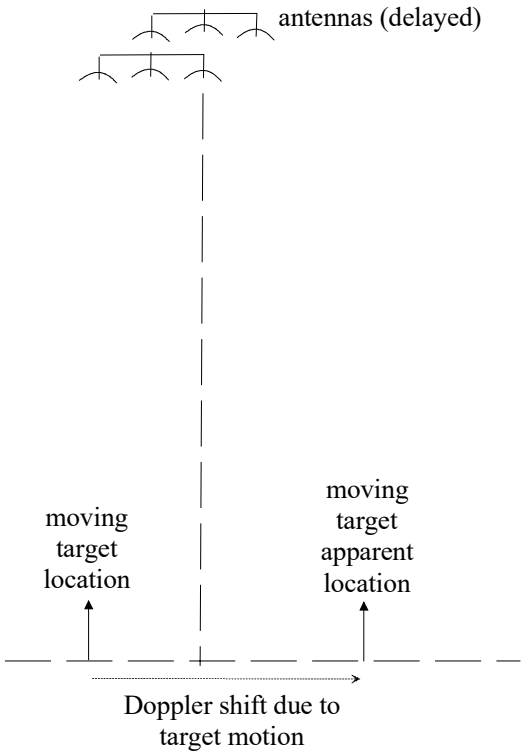

Figure 5. Three Phase-Center Delayed Interferometer

We now look at the IFSAR case from Figure 3 in a manner similar to the delayed interferometer case just mentioned for GMTI. Instead of delaying, we will "shift" the phase-center pairs by signal processing. We will assume that we know the location of target P1. In the absence of noise, we can develop a situation similar to the previous case for GMTI by "shifting" the interferometers and subtracting. The "shifting" and subtracting operation, in this case, becomes the steering of a null at the target P1. The interferometric signal after these operations can be shown to be:

$$X = \exp\left\{ j\frac{2\pi}{\lambda}\left(B_2 - B_1\right)\left(\sin\theta_2 - \sin\theta_1\right)\right\}\frac{\sin\left[\frac{2\pi}{\lambda}B_2\left(\sin\theta_2 - \sin\theta_1\right)\right]}{\sin\left[\frac{2\pi}{\lambda}B_1\left(\sin\theta_2 - \sin\theta_1\right)\right]} \tag{2}$$

Given that we know the location of the target P_1 and the baseline lengths, we can solve Eq. (2) for the location of target P_2.

In the above discussion, we have assumed that we know the location of one of the targets. In this case the target location is relatively straight forward. Unfortunately, unlike the GMTI case, the IFSAR case cannot make this assumption. Even more unfortunate is the fact that the problem of locating both targets is a much more complicated problem. If the location of one of the targets, either P_1 or P_2, is not known, the problem requires steering two nulls simultaneously until the total return is minimized. This problem is non-linear and there are multiple local minimums. In order to determine the overall global minimum requires a full search of two-dimensions for the two-target case. In general, the search requires an N_s-dimensional search of the array response for N_s -targets. This problem is very important in signal processing; however, it is an expensive problem in terms of computation. Many, many articles have been written about this problem and much effort has been spent on it. We will discuss some of the approaches in the next section.

CURRENT STATE-OF-THE-ART

Most of the current literature available in this area focuses on the general spectral estimation problem [10, 12]. Certainly, the problem we are dealing with in this LDRD is strongly related to the general spectral estimation problem. The problem is that the current literature tends not to include issues specific to IFSAR, such as baseline decorrelation, and speckle. The exception to this is the [9]. Also, the focus on generic solutions tends to overlook any simplification that might be available for the very important two-target problem case.

Spectral Estimation and Resolution

The spectral estimation problem is concerned with obtaining the estimate of the signal spectrum in the presence of interference. Often it is assumed that we have multiple sinusoids in Gaussian noise. In the case where the separation of sinusoids is greater than the Rayleigh resolution limit, the maximum likelihood estimator becomes a periodogram [10], i.e., the standard Fourier transform image formation that is typically done in SAR. In array terminology, the equivalent of the periodogram is typically referred to as "beamforming". These techniques are also referred to as non-parametric methods because they do not rely on assuming a particular form of received data. These are as opposed to parametric methods that will be discussed below.

The problem with beamforming in IFSAR is that the Rayleigh resolution is essentially equivalent to the ambiguous angle of the largest baseline for the system. For RTV, our Rayleigh resolution was about 100 m in height. If we rely on Rayleigh resolution for angular position measurement, we need to have very large antenna separation, (large baselines). For RTV, we would have needed about a 60 m baseline (about what was used on the space shuttle) for the Rayleigh resolutions that would approach the IFSAR performance we achieved in RTV.

We mentioned above the existence of parametric methods. The parametric methods assume a model for the received signal, such as multiple distinct sinusoids in Gaussian noise. If the model is correct, we have additional information that permits us to improve the resolution of two closely spaced signals and reduce surrounding interference. As a real simple example, assume that we have a single sinusoid in Gaussian noise. The non-parametric technique would involve forming the Fourier transform with the appropriate window function. The result would be a function that has the form of the Fourier transform of the window function shifted by the frequency of the sinusoid. The Rayleigh resolution is proportional to the time between the first and last samples. In the parametric method, we would take advantage of the fact that we know a priori that the desired signal is a single sinusoid. Then the problem becomes estimating the parameters of the sinusoid, such as its frequency, amplitude, and initial phase. In IFSAR, we typically focus on the spatial frequency estimation. The resolution of this frequency estimate is a function of signal-to-noise ratio, in this case. The ML estimator for this case is to interpolate to find the peak of the periodogram (under the condition that the amplitude of the sinusoid is unknown) [10]. In IFSAR, we use the phase of the maximum likelihood estimator for the complex correlation between the two phase centers to resolve the spatial frequency beyond the Rayleigh resolution limit.

Maximum Likelihood Estimation for Sinusoids in Noise

The maximum likelihood (ML) method for multiple sinusoids in noise is presented in [10, 11]. The derivation of the ML estimator for multiple sinusoids in noise is given in the appendix to facilitate understanding of the concepts that will be presented.

The main problem with the maximum likelihood estimator for multiple sinusoids is that the solution is highly non-linear and requires a search for a global minimum unless the signals are spaced far apart, as mentioned above.

In [10], the non-linearity of the ML estimator is shown via an example of two closely spaced sinusoids in the absence of noise. We will repeat that example shortly, but first we will separate the sinusoids a bit more to start out with. The form of the sinusoids is given in the following equation.

$$x(n) = \exp(j2\pi f_1 n) + \exp(j2\pi f_2 n + j\phi) \tag{3}$$

The first case we examine is when the separation of the targets is greater than the Rayleigh resolution. Figure 6 shows the results of the ML estimator when $f_1 = 0.5$, $f_2 = 0.65$, and $\phi = \pi/4$.

We note from Figure 6 that if we search for a local maximum in the wrong place, we will arrive at the wrong answer. In Figure 7, we project the 2-D figure to 1-D frequency (search space). The result is that the peaks are separated well enough in this instance that a 1-D Fourier transform would be adequate. In fact, as noted above, the ML estimator becomes the periodogram when the sinusoids are separated adequately.

The next case we examine is when the sinusoids are closer in frequency than the Rayleigh resolution. Figure 8 shows the results of the ML estimator when $f_1 = 0.5$, $f_2 = 0.52$, and $\phi = \pi/4$. Figure 9 shows the projection into 1-D frequency. Again, we have ignored noise. Notice that in this case there is very little separation between the peaks. It is especially difficult to tell in the projection into 1-D frequency. It would be even more difficult if the figure did not include shading and an artifact meant to keep the calculation from dividing by zero. The shading and artifact make the separation of the two sinusoids much more discernable in the figure.

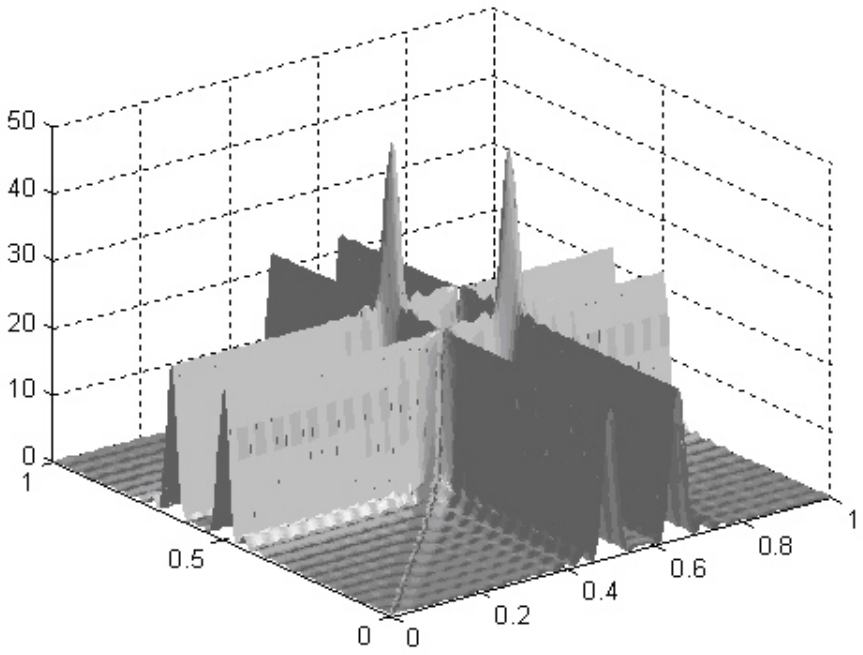

Figure 6. ML Estimator for Two Well Separated Sinusoids Without Noise

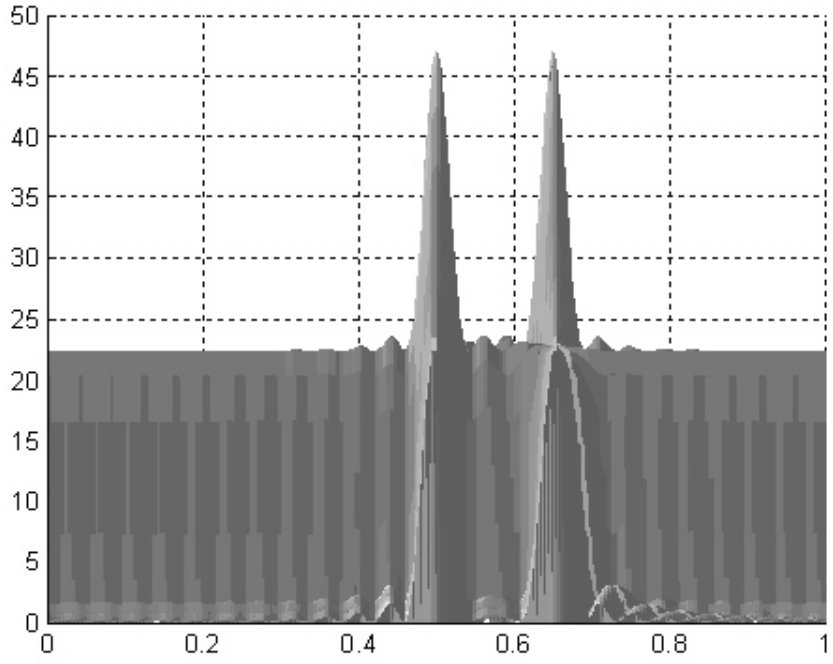

Figure 7. Previous Figure Projected into 1-D Frequency

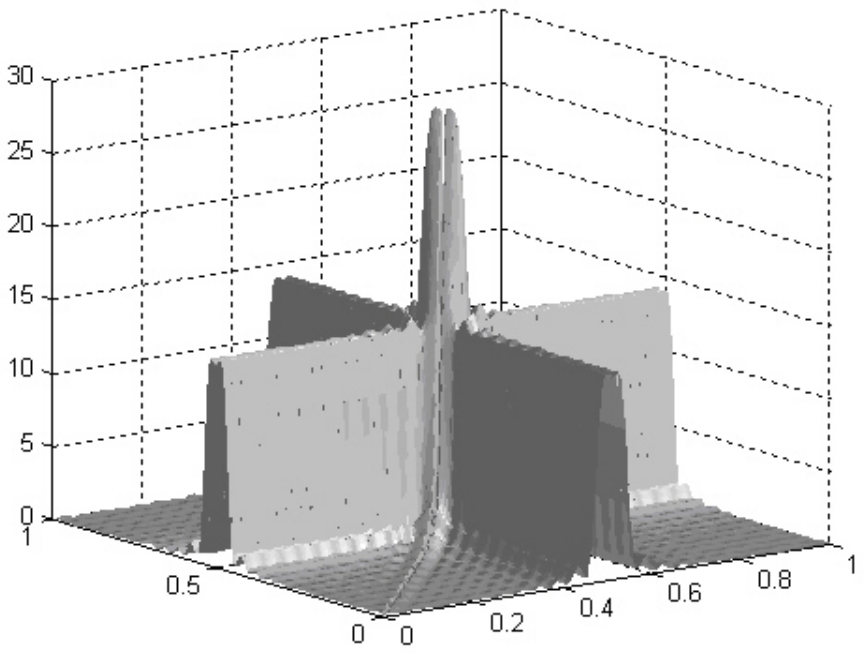

Figure 8. ML Estimator for Closely Spaced Sinusoids Without Noise

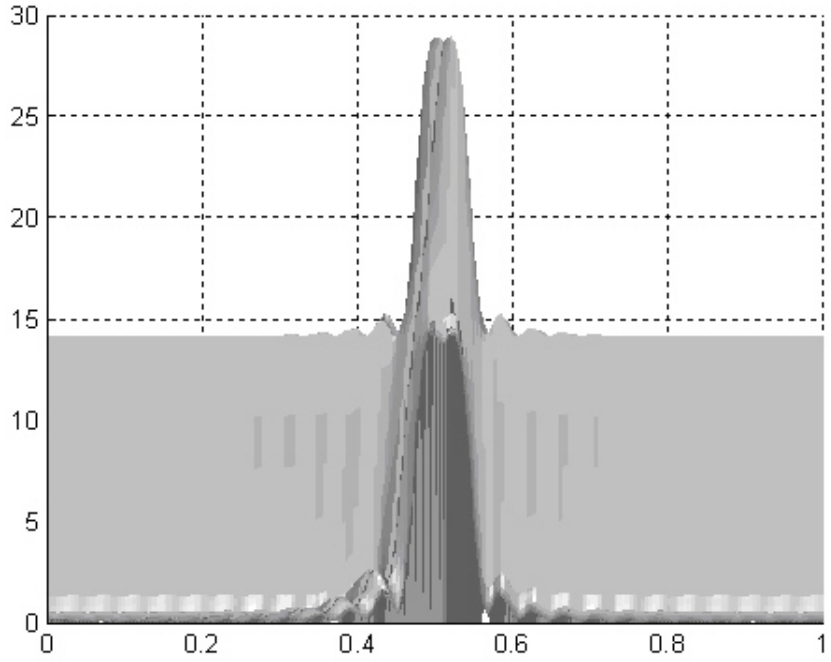

Figure 9. Projection of Previous Figure into 1-D Frequency

Non-Optimal Methods

Since the problem of estimating sinusoids that are closer together than the Rayleigh resolution is so important, much literature has been written on the subject. In addition, because the ML method is very computationally expensive, a lot of the literature tends to focus on suboptimal approaches. The suboptimal approaches attempt to trade performance for simpler processing algorithms. What these algorithms are willing to sacrifice is the ability to estimate frequencies noisy environments and/or with closely spaced sinusoids. Also, these algorithms sometime give up the guarantee of convergence to the global solution.

There are two typical main methodologies used in the above simplification for the problem of multiple closely spaced sinusoids in noise. The first approach attempts to simplify the search for the global solution. Many of these algorithms attempt to simplify the multidimensional search to a one-dimensional search. The second approach has become very popular and uses subspace methods. The former includes methods such as CLEAN [13], RELAX [14], and Alternating-Projection (or AP) [11]. The basic idea behind these techniques is that we try to iterate and eliminate one prominent signal at a time. The latter approach includes MUSIC, Min-Norm, ESPRIT, and other subspace algorithms.

Approximations to ML Methods

For our purposes described in this document, it is not clear that these techniques that attempt to simplify the global search are very useful. The CLEAN algorithm is known to require significantly more phase centers than incoming signals [15]. The AP technique requires equally spaced antenna phase-centers. The only one of these techniques that appears to show promise is the RELAX technique. In simulations the RELAX technique, as extended to multilook IFSAR, showed promise [16]. However, in practice with an actual system, the success observed in the simulation was not repeated [17]. Although we did not focus on the RELAX algorithm in this report, it is probably still worth considering in the future.

Subspace Methods

The next method mentioned above relies on the separation of signals from noise via subspace methods. The two things that really thrust the subspace methods into popularity is the simplicity of the numerical calculations when compared to the ML problem, and the fact that subspace methods will eventually achieve the optimal results given enough data. The subspace methods are suboptimal in that they do not converge to the CR-bound solution nearly as rapidly as the ML estimator. This leads to subspace methods requiring relatively high SNR for a given amount of data, when compared to other techniques. Nevertheless, simplicity counts for a lot and the techniques have been studied at length. The main interest in this report on the subspace techniques is that it will has been shown in [17] that the techniques can be used in practice and yield higher resolution than beamforming techniques under the right conditions [12].

There are several popular subspace algorithms. MUSIC [18] is the most popular and there are many variants of it. Root-MUSIC is very popular, but requires equal spaced samples because it solves for the roots of a polynomial. In this report, we will consider spectral MUSIC, because it

permits more general array geometries. The performance of spectral MUSIC is not quite as good as root-MUSIC, and unlike root-MUSIC, it requires a 1-D search.

Another subspace method that is similar to MUSIC is the Min-Norm [12] method. It is based upon linear prediction and also requires equal spaced samples.

A final subspace method that we will briefly mention because it is popular in literature is the ESPRIT [19] method. The ESPRIT method will not be considered here because it requires pair-wise symmetry in the array and requires twice as many elements for a given number of signals. The cost in the number of elements yields some performance improvement.

Derivation of MUSIC

We repeat the derivation of the MUSIC algorithm from [20] here, simply so that this report is self-contained. This development closely follows the development in [21].

Assume that the correlation matrix obtained from Eq. (39), *R*, for an array of antennas can be described by the following equation:

$$R = APA^H + \sigma_n^2 I \tag{4}$$

where

P = a diagonal matrix containing the signal power information from S
A = a matrix $A(\Theta)$ discussed in the appendix
I = identity matrix
σ_n^2 = the variance of the noise

Eq. (4) assumes there are N_s different target locations and K different phase centers, and that $N_s < K$.

For the correlation matrix in the form shown in Eq. (4), it can be shown that the N_s largest eigenvalues are $\sigma_{s,i}^2 + \sigma_n^2$ and the rest of the eigenvalues are σ_n^2, where $\sigma_{s,i}^2$ is the signal power for the i^{th} target. It is important to note that the eigenvectors corresponding to the N_s largest eigenvalues span the signal subspace. The rest of the eigenvectors correspond to the smallest eigenvalues and are orthogonal to the signal subspace. (Refer to [10] for discussions of both of these properties.)

The eigenvalue/eigenvector equation for the correlation matrix can be written as:

$$(R - \lambda_i I) q_i = 0 \tag{5}$$

where

q_i = the i^{th} eigenvector of the correlation matrix

λ_i = the i^{th} eigenvalue of the correlation matrix

For the $\left(K - N_s - 1\right)$ smallest eigenvalues (where $\lambda_i = \sigma_n^2$), the eigenvector equation becomes:

$$\left(R - \sigma_n^2 I\right) q_i = 0 \tag{6}$$

Substituting Eq. (6) in Eq. (4), yields:

$$APA^H q_i = 0 \tag{7}$$

It is very important to note that Eq. (6) and Eq. (7) are only appropriate for the eigenvectors that correspond to the noise eigenvalues. Assuming that there is no correlation between the target frequencies in the A matrix, then:

$$a_i^H q_i = 0 \tag{8}$$

where

a_i = the i^{th} column vector from the $A\left(\Theta\right)$ matrix

Eq. (8) is the key to the MUSIC algorithm. It says that we estimate the signal subspace as orthogonal to the noise subspace. What Schmidt did in [18] was to note that the noise subspace is orthogonal to the signal subspace and to take advantage of this fact.

In a noisy environment, Eq. (8) does not hold exactly. Therefore, the MUSIC algorithm estimates the frequencies by looking for the N_s peaks in the following function:

$$f\left(\omega\right) \approx \frac{1}{\sum_{i=L+1}^{M} \left| a_i^H q_i \right|^2} \tag{9}$$

It is very important to point out that Eq. (9) is not a true spectrum. It is referred to as a "pseudo-spectrum", because, as we will see later, the amplitudes of the peaks in Eq. (9) have very little correlation with the true amplitudes of the spectrum. MUSIC only estimates the frequency of the sinusoids and must be used in conjunction with some other algorithms to determine amplitudes. We will show examples of this later.

Another key point is that MUSIC, as well as most other techniques we have discussed so far, require an estimate of the number of sinusoids present. Discussion of this is presented in the section on model order.

Eq. (9) is referred to in literature as spectral MUSIC. It has been noted [23] that if the samples are equal spaced, then Eq. (8) can be solved for the roots that are nearest to the unit circle. This is termed the root-MUSIC method in literature.

The practical difficulty with MUSIC and Eq. (9) is that in practice, we often have no a priori knowledge of the correlation matrix. We must estimate the correlation matrix from noisy data. The result is spurious peaks in Eq. (9) and suboptimal performance at low SNR.

It should be pointed out that for the case where there is one less signal than there are sensors, the MUSIC algorithm becomes the Pisarenko harmonic decomposition (PHD) algorithm [22].

Geometric Interpretation of Subspace Methods

In [Schmidt], there is a very clever geometrical treatment of the problem of antenna arrays and subspaces. The treatment and terminology derived from this treatment is commonly found in literature. We will attempt to make this geometrical interpretation accessible in the following discussion. We will follow [18, 19] in this presentation.

In the appendix (on ML), the signal received by the antenna was modeled in Eq. (39) as:

$$X = A(\Theta)S \tag{10}$$

It is very important to this development to note that we are ignoring noise from Eq. (39).

In this model, the array response to targets at angle Θ is included in $A(\Theta)$. $A(\Theta)$ are vectors from the set of all steering vectors that describe how the array responds to targets at all angles [19]. Note that we are assuming for now that the array response is only a function of one target angle, Θ. This implies that the phase centers for the array are contained along a line and have ideal behavior. The assumption that the array response is a function of only one variable means that the response can be visualized as a curve that "snakes" around in space. This curve must, at least, connect to itself at when Θ is 2π radians. This curve is referred to as the "array manifold" because in the general case where the array phase centers are not along a line, the response is a more complex surface that can be described mathematically as a manifold [24]. Array performance and ambiguities can be described in terms of the array manifold [18, 24] but we will not consider that in this report. Figure 10 shows a cartoon of a made-up manifold.

Since the array manifold describes the response of the array, Eq. (10) says that the signal received at the antenna is the superposition of scaled (by S) steering vectors along the array manifold. The specific steering vectors in Eq. (10) are those vectors, chosen from the array manifold, which correspond to the direction of the targets viewed by the array. Therefore, the number of steering vectors that are combined to make up the received signal is equal to the number of targets viewed by the array. Notice that the columns of the steering matrix $A(\Theta)$ are made up of select vectors (i.e., the vectors for the directions of the targets) chosen from array manifold.

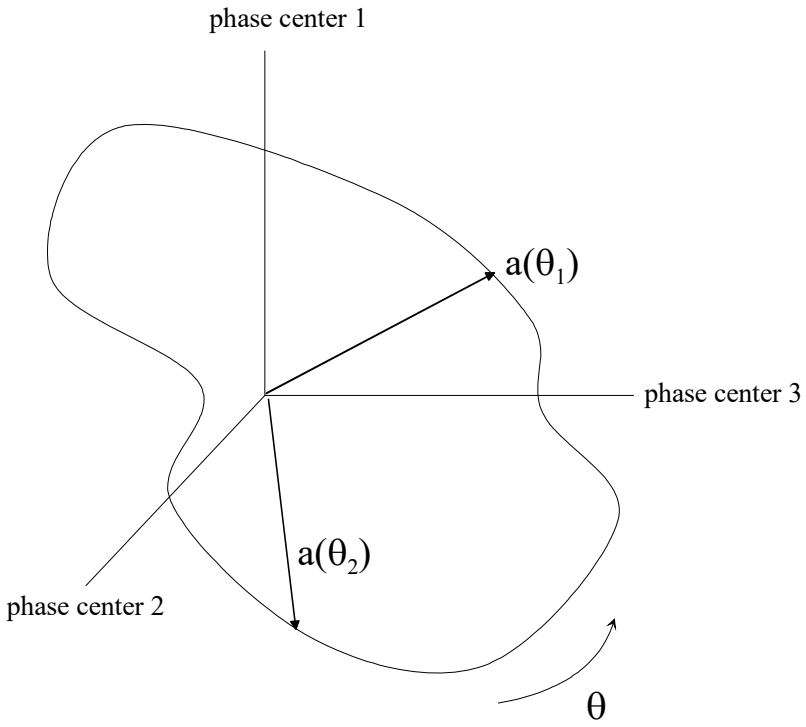

Figure 10. Geometrical Interpretation of the Array Manifold for Linear Array.

At this point, we take a chance that we will repeat ourselves, and risk boring the reader because it is important to make this point. Again, Eq. (10) says that in the absence of noise the solution is a superposition of the vectors from the columns of $A(\Theta)$, which in turn come from the array manifold. The number of columns in $A(\Theta)$ corresponds to the number of distinct target directions that are present. Let the number of distinct signal directions be N_S, then Eq. (10) says that the solution is contained in the N_S-dimensional subspace "spanned by the columns of $A(\Theta)$" [19]. (A good reference on subspace is [25].) This subspace is referred to as the signal subspace [18]. Eq. (10) says that the solution is the vectors contained in the intersection of the signal subspace with the array manifold. It is critical to note that we are still talking about the case where there is no noise present. The following picture illustrates the geometrical interpretation of Eq. (10). In the figure, we assume there are two targets present, i.e., $N_S = 2$. In this case, the signal subspace becomes a plane. The intersection of the signal subspace with the array manifold is shown in Figure 11 below. The solution from this intersection are the vectors $a(\theta_1)$ and $a(\theta_2)$.

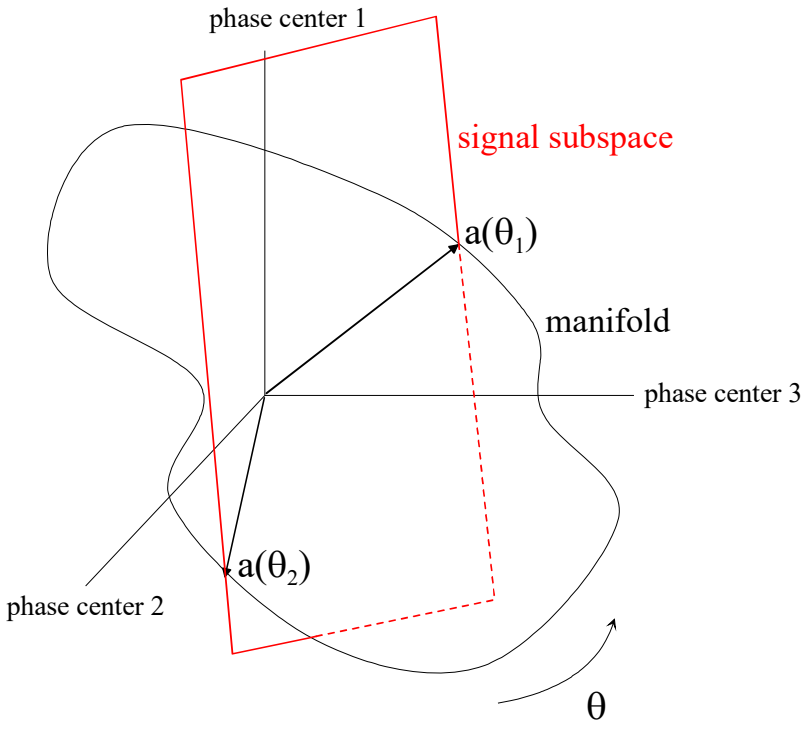

Figure 11. Geometrical Interpretation of Target Location and Signal Subspace Methods

The next step is to add noise to this interpretation. We then get the equation from the appendix:

$$X = A(\Theta)S + N \tag{11}$$

The ML method says that in the presence of noise, N, we attempt to find the combination of vectors along the array manifold that best fit the noisy data, X. It is apparent that this involves an N_s-dimensional search of the nonlinear array manifold. This leads to the complexity of the ML method.

The geometric interpretation of the subspace methods is now presented. In subspace methods, we attempt to estimate the best fit subspace given the data. Then we attempt to find the points of closest approach of this subspace to the array manifold. This approach is suboptimal, in that it does not achieve the ML performance in low SNR situations. However, as the amount of data available for the estimate becomes infinite, the error in the estimate of the subspace reduces, and the subspace solution approaches the correct (noiseless) solution. Therefore, subspace solutions do converge to the correct solution. This is one of the nice properties of the subspace techniques that have led to their popularity.

As a caution, we have shown figures that correspond to real, rather than complex, signals because they are easier to draw and visualize. In truth, the array manifold; hence $A(\Theta)$ and the signal subspace, are complex values and should be treated as such.

Array Interpolation Methods

Array interpolation methods (e.g., [26]) enable us to use methods that require equal sample (or some other constraint on) spacing for arrays that do not have equal sample spacing. For example, array interpolation would allow us to use root-MUSIC, Min-Norm, Alternating Projection, or ESPRIT. The methods that require equal sample often have some slight performance benefits over those that do not have this constraint. The additional cost of array interpolation is that the interpolation is only valid over a small range of angles of the target; therefore, new sets of interpolation functions are required to cover the entire range of angles. The range of angles depends upon the desired performance. A tighter range of angles will yield better position performance.

Beamforming and Non-parametric Techniques

This section briefly touches upon tomography, beamforming, and nonparametric techniques. Much of the material here follows from [12]. Traditional beamforming, as mentioned earlier, is the spatial counterpart to the periodogram in time-series analysis. The beamformer attempts to pass signals from the desired direction while at the same time attenuating signals from all other directions under the assumption that the signals from the other directions are spatially white. The beamformer has the resolution of the Rayleigh resolution limit and the familiar sidelobes due to spectral leakage. The beamformer concept is common to standard far-field SAR processing. The beamformer is a non-parametric technique, meaning that it does not assume a priori information is available about the spatial spectrum of the signal.

The beamformer is not the only non-parametric method available. Another common one is Capon's method. There are several variants on Capon's method, but essentially this method attempts to pass through the signal from the desired direction while attenuating signal that the array detects from other directions. The difference from the beamformer is that Capon's method is "data dependent" [12]. "It produces better resolution and lower sidelobes than the beamforming method by adaptively rejecting spectral components different from the current filtered spatial frequency." [9]. As noted, the achieved resolution and sidelobe performance are potentially better than the beamforming method. The cost is that the correlation matrix must be known or estimated. Capon's method achieves better resolution than beamforming, but worse than MUSIC. Capon's method is meant to be a true spectral estimator, but typically has poor amplitude estimation performance. This has led to many variations to this algorithm published in literature. The Capon's method is used quite a bit by the Europeans, and should be considered in future investigations because it tends to work better in low SNR environments than does MUSIC.

In the case where the far-field assumption is not quite adequate, especially for large baseline, focusing is required. Typically, when focusing is required the 3-D imaging is referred to as tomographic processing [27, 28, 29, 6]. The focusing may be quite simply the standard quadratic focus vector [6, 29]. It should be noted that any of the techniques mentioned in this paper could be used to form the 3-dimensional images required. The authors tend to think of focusing different height slices as true tomography through traditional beamforming, as in [28]. If we pick a few angles to focus on, this does not address the issue of height estimation. However, if enough slices are processed, it does lead toward true 3-dimensional imaging.

The question of which of the above method to use is a complex trade-off of several factors. These factors include, but are not limited to: the array size (e.g., baseline length); the required processing; the performance of the method; the spatial resolution desired; is the data sparse in the angular direction; is the array sparse; etc.

Maximum Likelihood and Extended Targets

The assumption that the targets observed by the radar system are sinusoids is not completely accurate. In literature, this is usually termed the "narrowband assumption" [30]. The narrowband versus wideband question is strongly related to baseline decorrelation in traditional IFSAR. The narrowband assumption says that we assume that the signal stays correlated across the entire array. For IFSAR this means that we can consider the signal to come from one specific direction, i.e., it behaves like a point target. In truth the signal come from all angles contained within the range-Doppler resolution cell. If the returns are sufficiently strong; the angular extent of the resolution cell large enough; and the baseline large enough, then the narrowband assumption does not hold.

In [30], it states that if "the effective rank of the signal subspace is larger than the number of signals present", we need to consider the signal a wideband signal. In IFSAR, this occurs when the signal correlation is due to baseline decorrelation and other issues is low. A good discussion of including baseline decorrelation effects is presented in [9]. One of the issues pointed out in [9] is that the terrain slope needs to be known to take into account the baseline decorrelation. For fairly flat terrain and modest baselines, the received signal can be considered narrowband. In the case where baseline decorrelation starts to become important for the largest baseline, the return signal cannot be assumed to be constant across the array. In this case we have a wideband signal.

MODEL ORDER

One of the key issues in direction-of-arrival problems is referred to as the "model order" problem. This is simply the estimation of how many signals are present. As discussed previously, the typical problem assumes constant amplitude sinusoids in noise. Parametric techniques, unlike non-parametric techniques, require a knowledge or estimate of the number of sinusoids present.

For this LDRD, we are focusing on the two-target case which simplifies matters. Assuming that there is at least one target present, we are left with two hypotheses: there is one target present; or there are two targets present.

In general, model order selection is a large topic. The name and the techniques come from dealing with the autoregressive model. A good discussion of these techniques can be found in [10, 12]. In the case of using subspace techniques or eigenanalysis techniques, we can test the eigenvalues of the cross-correlation matrix against a threshold to estimate the number of signals present [10].

For IFSAR there are a couple of interesting methods that use information available through standard IFSAR processing. One of the methods assumes that the noise power in the image is known. The other assumes that the smallest baseline is quite small.

The former method has been used extensively for detecting volume decorrelation in IFSAR systems from vegetation [31]. This method presumes that decorrelation in the IFSAR sensor is generally dominated by thermal noise. Then we can use the fact that a "spread" in targets within a resolution will allow cause decorrelation beyond just thermal noise. The detection of target spread is accomplished by the following:

$$\frac{\mu}{\hat{\mu}_{snr}} = \hat{\mu}_{geom} < threshold \tag{12}$$

where

μ = correlation estimated from the data

$\hat{\mu}_{snr} = \frac{\hat{snr}}{\hat{snr}+1}$ = estimate of correlation component due to SNR

$\hat{snr}$ = estimate of the SNR (unitless)

$\hat{\mu}_{geom}$ = estimate of geometric decorrelation due to "spread" of target

Certainly, since Eq. (12) is a ratio, it can be written in terms of logarithms and the threshold could be specified in deciBels.

A similar method would be to use the ratio of the correlations between the large and small baseline. If the signal-to-noise ratios are the same for each image, the correlation due to thermal noise cancels. The corresponding threshold for this method is reduced by the baseline decorrelation of the smaller baseline.

As mentioned above, another simple technique proposed in [10] under the assumption that the sources are narrowband, is to test the eigenvalues of the correlation matrix against a threshold related to the expected noise. One advantage of the correlation threshold technique over the eigenvalue method is that we do not need to calculate the eigenvalues of the correlation for each pixel. The correlation, presented above, comes as a natural product of traditional IFSAR processing, so it is available at no extra cost. We could use the correlation to select only those areas likely to have multiple targets and only perform the estimation of the two frequencies on those targets.

METHODS INVESTIGATED

Because of the various issues mentioned above, this report will focus on two different approaches. The first approach uses spectral MUSIC combined with the amplitude estimation from the appendix. The second approach attempts to solve the equations for the case of two sinusoids. The rest of this report will discuss these approaches.

SUBSPACE APPROACH

By process of elimination, the spectral MUSIC technique appears to be a reasonable candidate for resolving closely spaced two-target problem in IFSAR. As noted above, MUSIC is not a true spectral estimator, and because of this it cannot estimate the amplitudes. As suggested in [17], we examined using the frequencies estimated by spectral MUSIC in the maximum likelihood estimate of the amplitude from Eq. (47) in the appendix.

SIMULATION AND RESULTS

A simulation that uses the spectral MUSIC and maximum likelihood amplitude was developed. The simulation extends the standard simulation of IFSAR data from the one-target to the two-target case. The simulation still assumes that the targets and the noise are circular-Gaussian distributions. The phase modulation, in the absence of noise, contains the range differences information. The simulator allows adjustment of the relative amplitudes of the two targets; the location of the two targets; the signal-to-noise ratio; and various radar geometry parameters, including baseline lengths. The simulation allows the number of looks to be an independent variable. The simulation assumes two targets and three phase centers. Currently the simulation assumes that there are always two targets present. It is *very important* to note that *all target separations considered in this section are well below the Rayleigh resolution limit* of about 100 m.

A simple example is presented to demonstrate the simulation and illustrate the limitation of using the MUSIC pseudo-spectrum. In this example, the small baseline is 0.1 m, and the large baseline is 0.3 m. The range is 8 km, and the grazing angle is 40°. The height of the first target is set to 0 m, and the second is set to 30 m. The SNR of the first target is 20 dB, and the SNR of the second target is 15 dB. The number of looks used was 30. The results of the MUSIC pseudo-spectrum are shown in Figure 12. The amplitude estimate is in Figure 13. There are a couple things to notice about the MUSIC pseudospectrum. First, the “amplitude” in the pseudo-spectrum does not correspond to the signal strength. The amplitude corresponding to the target at angle 0º is actually 5 dB brighter on the average than the other target. From the pseudospectrum in this example, it appears the opposite is true. In general, the amplitudes from the pseudo-spectrum appear to be random and have little correlation with the true amplitudes. The estimated heights from MUSIC in this example are -1.7 m and 39.5 m.

The above illustration is meant to show that the MUSIC spectral estimator only estimates frequencies and must be used in conjunction with another estimator to estimate the amplitudes of the signals. The example above is common but not typical. A more typical result is shown below in Figure 14 and Figure 15.

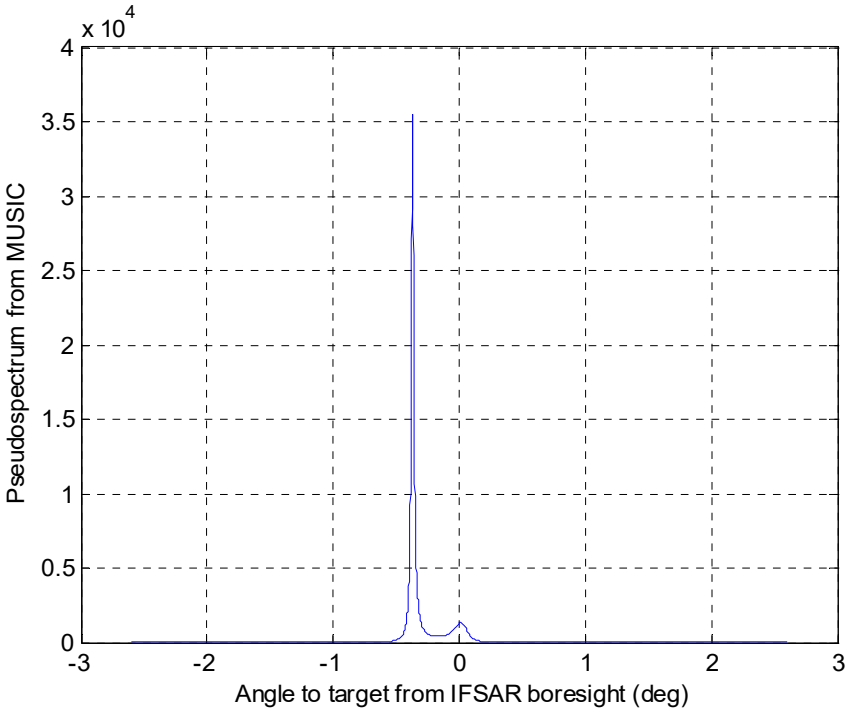

Figure 12. Example MUSIC "Pseudo-spectrum"

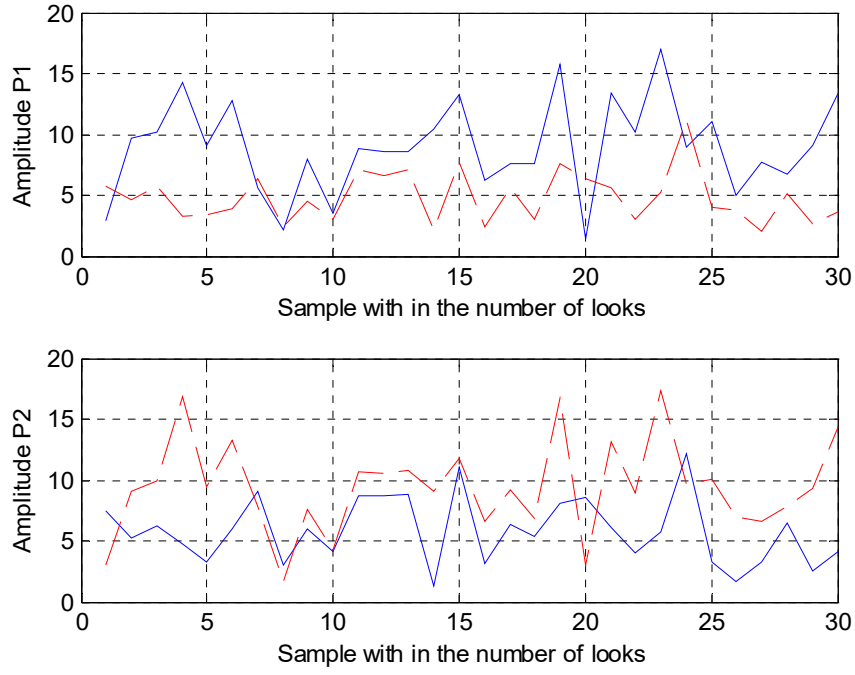

Figure 13. Amplitude Estimates from ML Method Assuming MUSIC for Frequency Estimation (Blue Actual Amplitude, Red Estimated Amplitude)

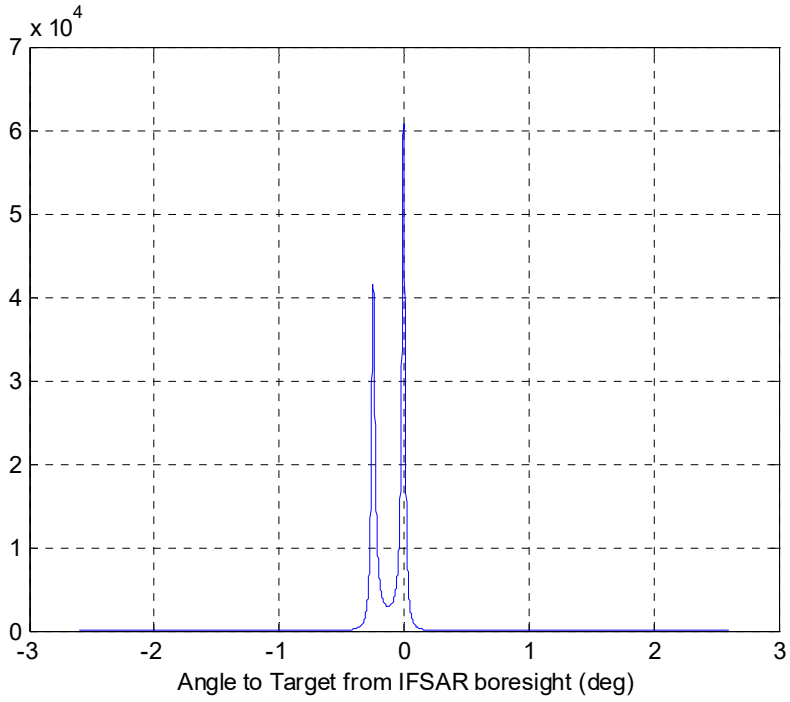

Figure 14. More Typical Example of MUSIC "Pseudo-spectrum"

Figure 15. Amplitude Estimates from ML Method Assuming MUSIC for Frequency Estimation for More Typical Case

Now we examine statistics using the same parameters presented above, except for this case we will assume that first and second target are equal strength and that both have an average SNR of 20 dB. Also, we will place the height of the second target to 50 m. The histogram of heights estimated for over 3000 trials by the above method is shown in Figure 16. The histogram shows a bell curve looking distribution centered around 0.2 m and 49.5 m. The standard deviation for the target at 0 m height is 2.6 m and the standard deviation for the target at the 50 m height is 2.5 m.

Before leaving this example, it is informative to show the results that would be achieved from traditional IFSAR processing from the largest baseline. Figure 17 shows the results from traditional IFSAR of the estimated height. Notice that the average value of the height estimated is nearly the average height of the two targets, 24.9 m. The distribution has a larger spread of about 4.4 m. Actually, we only get the average height of the two targets for the case where the targets have the same average intensity [7]. In general, the height favors the brighter target. Also note that the distribution has more spread. This will be used to advantage in the section on model order.

Notice that the figure for traditional IFSAR processing appears to show a height distribution which is not multimodal, as in the MUSIC case. We emphasize here that traditional IFSAR is a parametric technique which assumes that there is only one target direction, i.e., spatial frequency, present. Traditional IFSAR processing achieves resolution much greater than Rayleigh resolution by estimating the frequency of a single sinusoid. The MUSIC technique assumed that there were two different target directions present; hence the bi-modal distribution.

Another comment should be made on the comparison of the single target versus two target height estimation. The height noise standard deviation for a single 20 dB SNR target would be about 0.6 m. This is significantly below the observed 2.5 m for the two-target case from this simulation. The comparison is really “apples and oranges”, because even though the noise is lower for a single target than in the two-target estimation case, the noise using traditional IFSAR processing for the two-target case is much worse than achieved with MUSIC.

Next, we vary reduce the angular separation between the targets to see how the algorithm responds. We repeat the above simulation for the second target at 30 m now, instead of at 50 m. The result of the height estimates illustrated in Figure 18. The distributions are centered at 0.5 m and 29.5 m. The standard deviations around this are 4.4 m for the lower target and 4.5 m for the higher target. Note that the distributions are closer together. Another thing that should be noted is that I could detect only one peak about 1.7% of the time. In this case, I ignored this data.[†]

[†] It should be noted that for this report, a reasonable threshold scheme was used to eliminate spurious peak; however, no attempt was made to optimize this threshold.

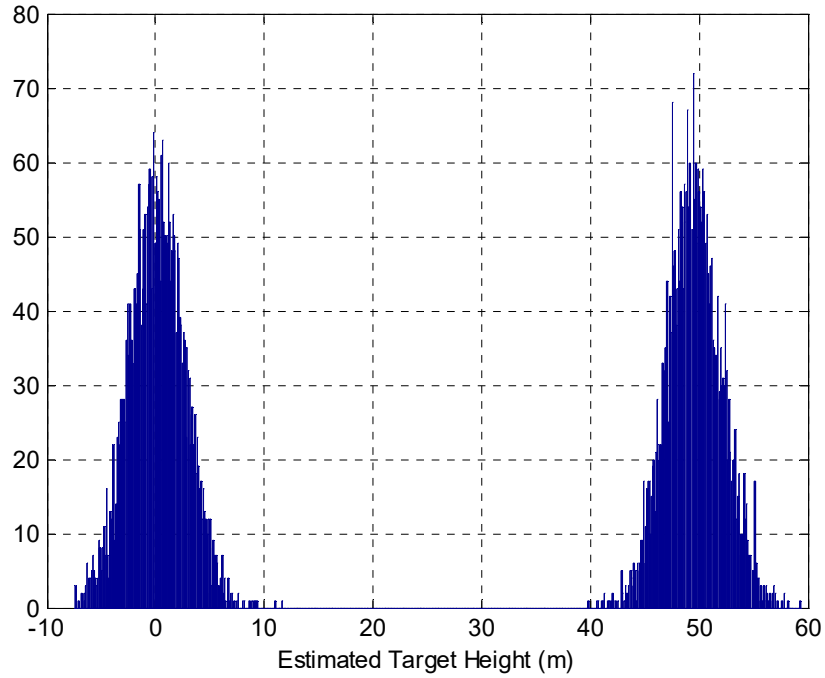

Figure 16. Histogram of Height Errors for Equal Target Strength and 50 m Target Separation via MUSIC

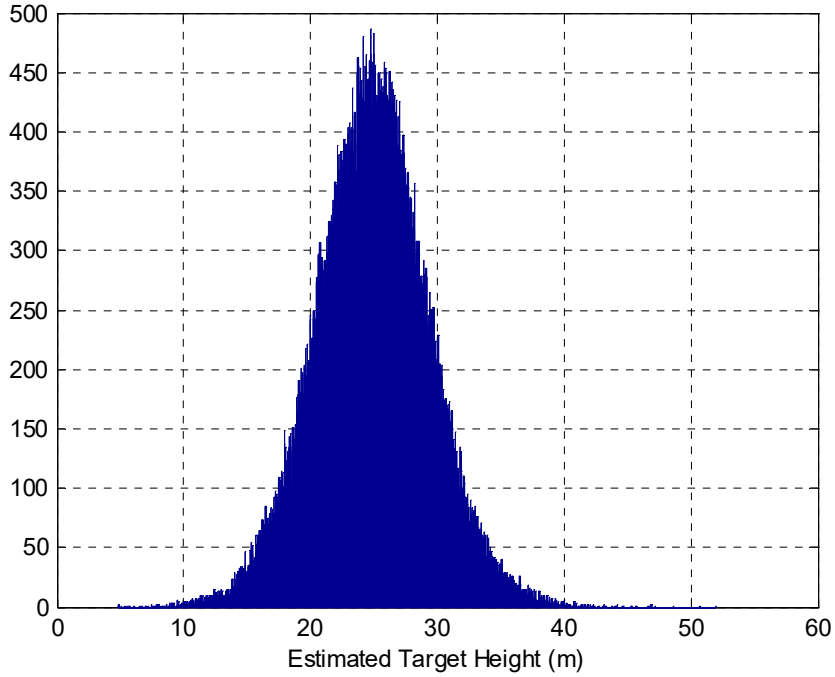

Figure 17. Histogram of Height Errors for Equal Target Strength and 50 m Target Separation via Traditional IFSAR

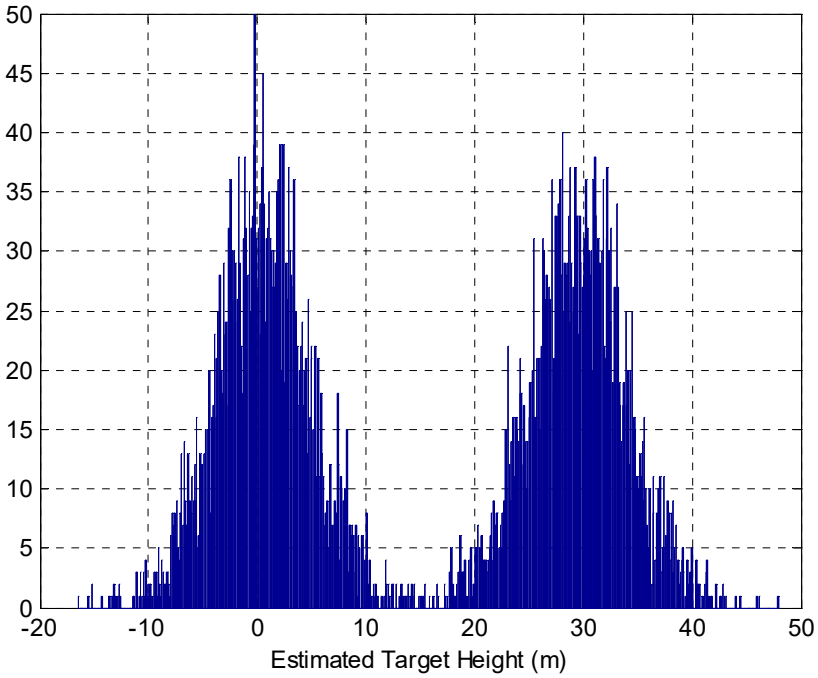

Figure 18. Histogram of Height Errors for Equal Target Strength and 30 m Target Separation

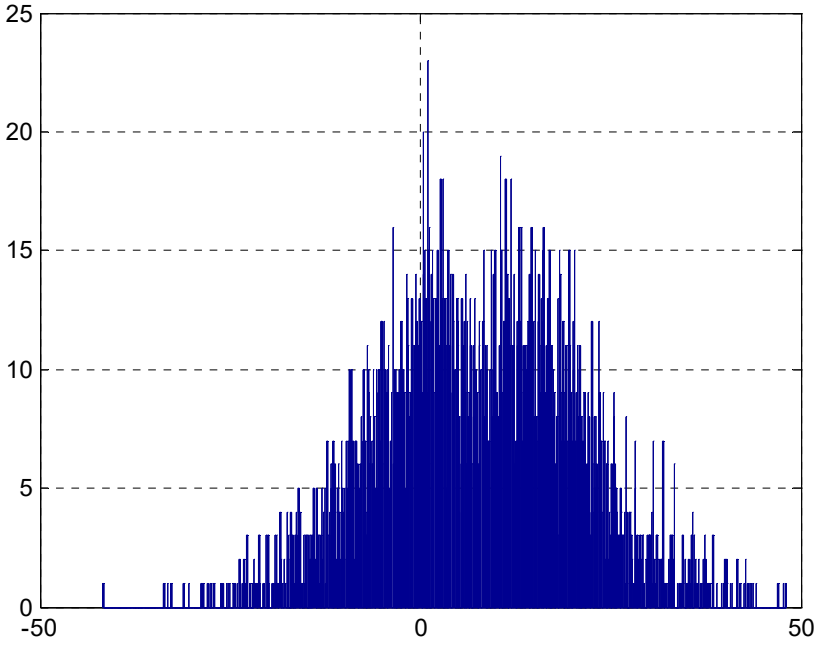

Figure 19. Histogram of Height Errors for Equal Target Strength (20 dB SNR) and 15 m Target Separation

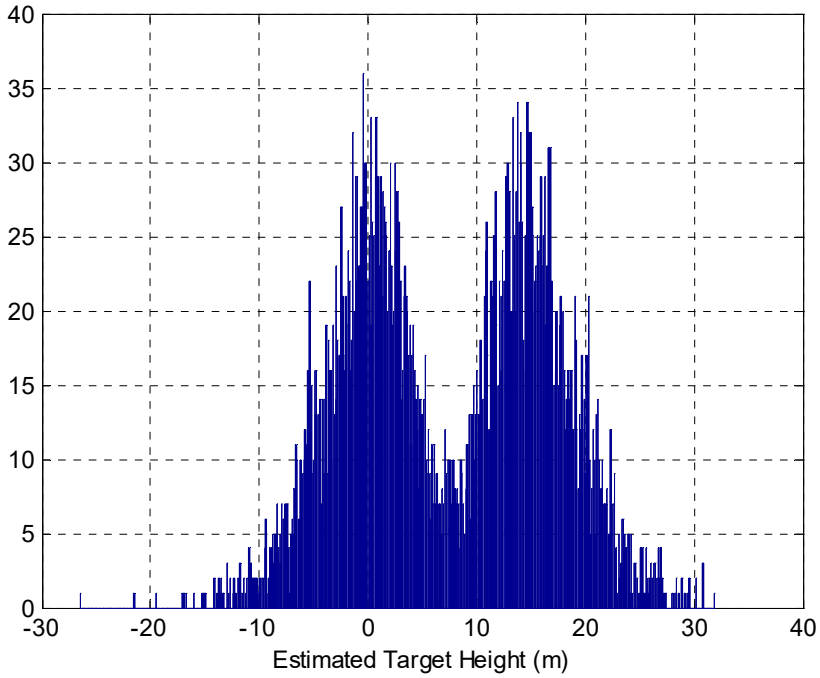

Figure 20. Histogram of Height Errors for Equal Target Strength (25 dB SNR) and 15 m Target Separation

We continue to reduce the angular separation and simulate setting the upper target at 15 m. In this case, 45.1% of the time only one target was found. The distribution of the remaining samples is presented in Figure 19. The distributions have merged in this case, and appear to be noisier. It is interesting that the loss of bimodal characteristics of the distribution coincides with the inability to find two peaks in the MUSIC pseudo-spectrum. The distributions are centered around -2.6 m and 17.8 m, respectively, and appear to have about a 7.8 m standard deviation. The standard deviation and mean are estimated assuming we can separate the distributions for the two targets, but we cannot.

Now, we increase the signal-to-noise ratio of both targets for the case where the two targets are separated by 15 m. The SNR is bumped up to 25 dB for both targets. The improvement is quite noticeable from Figure 20. The separation between the distributions is visible again. The average peaks of the distributions are at -0.4 m and 15.4 m respectively, with an apparent standard deviation around each peak of about 4.4 m.

We adjust the simulation to examine what happens when both targets do not have the same intensity. For this case the height is set back to 30 m, but the targets are set to 20 dB SNR for the target at 0 m height, and 15 dB SNR, for the target at 30 m height. The height distribution is shown in Figure 21. The average height for the lower target is 0.1 m and the average height for the higher target is 29.4 m. The standard deviation for the lower target is 4.3 m and for the higher target is 7.7 m. Notice that the higher target is also 5 dB less in SNR than the lower target. The percent of the time that only one target was found has grown to 9.1%.

The effect of number of looks is investigated by repeating the previous simulation while increasing the number of looks from 30 to 100. The results are shown in Figure 22 for this case. The percent of only one target is about 0.1%, for this case. The average estimated height is 0.2 m for the lower target and 29.1 m for the higher target. The standard deviation has improved to 2.4 m for the lower target and 4.5 m for the higher target.

The small baseline is reduced in the simulation. For this, we go back to 30 looks and both targets having 20 dB SNR. Figure 23 shows the histogram. In this case, we reduce the small baseline to 0.0375 m. The percent of one target only detections is 23.3%. The average estimated height for the lower target is -0.7 m, and 30.7 m for the higher target. The standard deviation is about 8.3 m for both the higher and lower targets.

The large baseline is increased. The same parameters as the previous simulation are used, except large baseline is 0.4 m and small baseline is 0.1 m. Figure 24 gives the histogram for this simulation. There were no single target detects. The average lower target height is 0.2 m, and the higher target is at 29.7 m. The standard deviation about 2.3 m for this case.

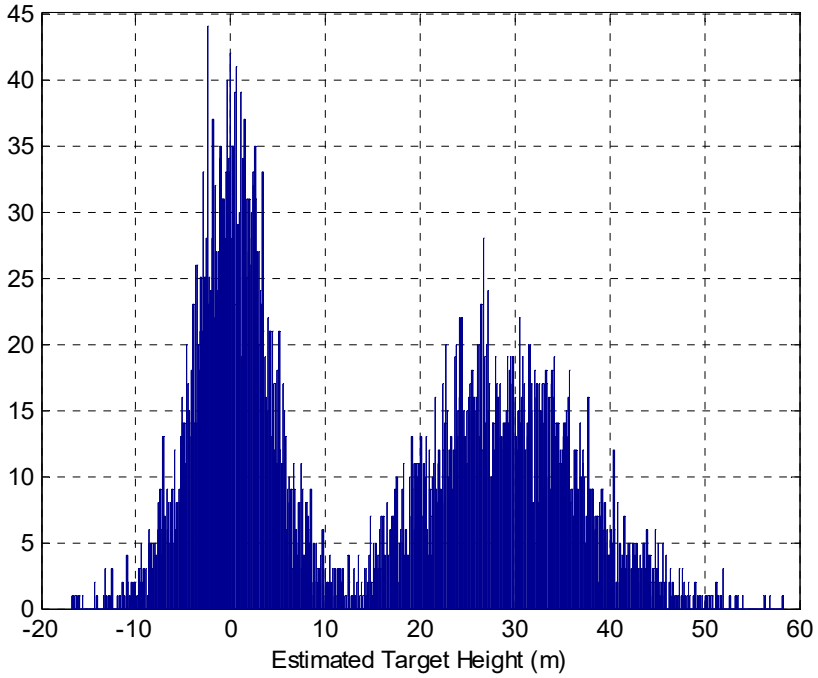

Figure 21. Histogram of Height Errors for 20 dB and 15 dB SNR Targets and 30 m Target Separation

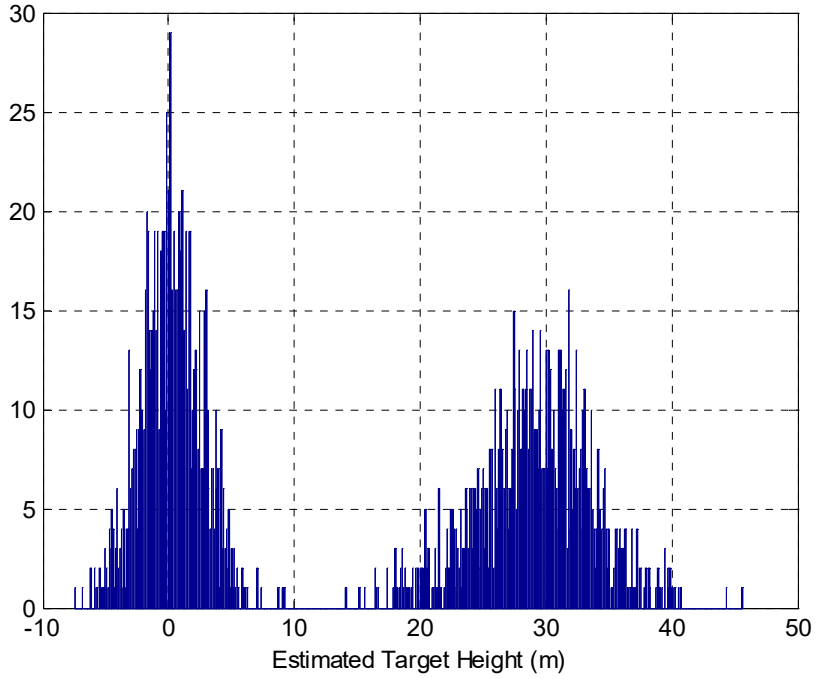

Figure 22. Histogram of Height Errors for 20 dB and 15 dB SNR Targets and 30 m Target Separation with 100 looks

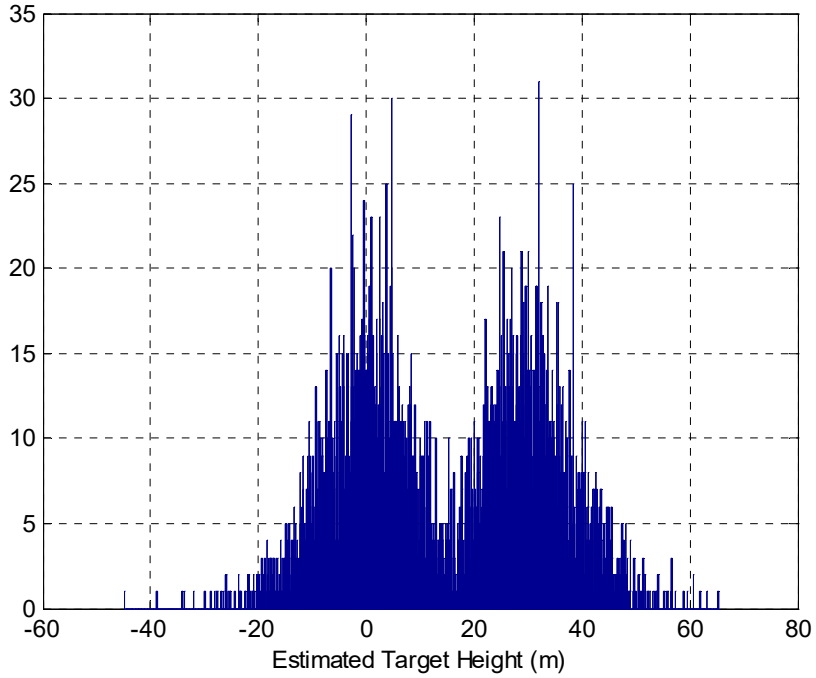

Figure 23. Histogram of Height Errors for Equal Target Strength and 30 m Target Separation Small baseline is 0.0375 m

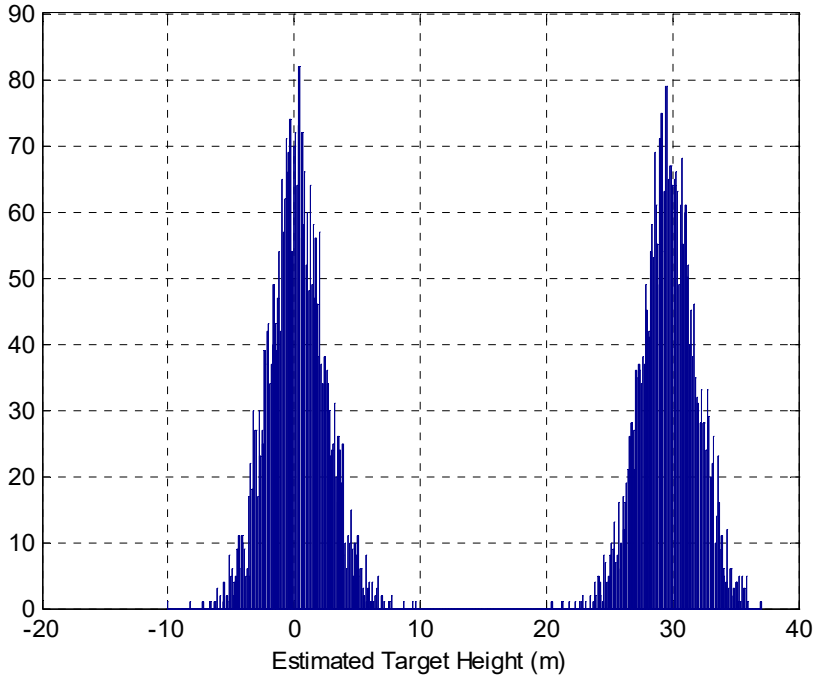

Figure 24. Histogram of Height Errors for Equal Target Strength and 30 m Target Separation Small baseline is 0.1 m and large baseline is 0.4 m

DIRECT METHOD

In this section we present a direct method for analyzing the SAR layover phenomenon involving two targets in a single range-azimuth resolution cell. The two-phase-center IFSAR assumes that each range-azimuth bin contains at most one target, but in scenes where the height changes abruptly, as is the case for some buildings, this technique suffers from SAR layover; the return signal is the superposition of two signals from two point targets, with different heights, that have been mapped into the same range bin, see Figure 3. We propose a direct method that uses a three-phase-center IFSAR to resolve this layover problem. Aside from its utility in solving the layover problem, the direct approach may also prove to be a useful tool for analyzing the resolution limit imposed by noise.

For the coherence factor, μ, that arises from a scene in which two-point targets reside in a single range resolution cell, the Van-Cittert Zernike Theorem yields,

$$\mu(k_l) = \frac{I_1}{I_1 + I_2}\exp(jk_l \sin\theta_1) + \frac{I_2}{I_1 + I_2}\exp(jk_l \sin\theta_2) \tag{13}$$

where

$\mu(k_l)$ = coherence factor for one pair of phase centers $(l = 1,2,3, \quad k_1 > k_2 > k_3)$, with

$k_l = 2\pi m B_l / \lambda_l$

B_l = baseline length

λ_l = center wavelength

θ_i = angle of arrival of the signal from point target at $\mathbf{p}_i$ (see Figure 3)

$I_i/(I_1 + I_2)$ = relative intensity of the point target at $\mathbf{p}_i$

m = 1 or 2, depending on whether the antenna is used in the standard mode or multiplex mode respectively

Here, we adopt the convention that the points in a cell are labeled in such a way that $2d = \sin\theta_2 - \sin\theta_1 \geq 0$.

In polar coordinates the coherence factor $\mu(k_l)$ becomes

$$\begin{aligned}\mu(k_l) &= \exp(jk_l s)\left[\frac{I_1}{I_1 + I_2}\exp(-jk_l d) + \frac{I_2}{I_1 + I_2}\exp(jk_l d)\right] \\ &= \left|\mu(k_l)\right|\exp\left[j\left(k_l s + t_l\left(\frac{I_1}{I_1 + I_2}, d\right)\right)\right]\end{aligned} \tag{14}$$

where

$$\left|\mu(k_l)\right|^2 \equiv \frac{I_1^2}{(I_1+I_2)^2} + \frac{I_2^2}{(I_1+I_2)^2} + 2\frac{I_1 I_2}{(I_1+I_2)^2}\cos(2k_l d) \tag{15}$$

$$t_l(\alpha,\beta) = \tan^{-1}\left[(1-2\alpha)\tan(k_l\beta)\right] \tag{16}$$

$$s = (\sin\theta_1 + \sin\theta_2)/2 \tag{17}$$

$$d = (\sin\theta_2 - \sin\theta_1)/2 \tag{18}$$

The unwrapped phase of $\mu(k_l)$ is given by

$$y_l = k_l s + t_l\left(I_1/(I_1+I_2), d\right), \qquad l = 1,2,3 \tag{19}$$

We show that the preceding equations are sufficient to enable us to solve for the three unknowns: *s*, *d* and $I_1/(I_1+I_2)$. We begin by presenting a criterion for detecting the presence of two targets, next we consider the case $I_1/(I_1+I_2) = I_2/(I_1+I_2) = 1/2$, and finally we examine the more difficult case $I_1/(I_1+I_2) \neq I_2/(I_1+I_2)$.

From the expression for the magnitude squared, we see that $\left|\mu(k_l)\right| < 1$ if and only if two targets are present in the same range resolution cell. Here, we assume that there are at most two targets in the same range bin. Also, assuming that two targets are present, it can be shown that for $k_l > k_m$,

$$\operatorname{sgn}\left\{\frac{k_m}{k_l}y_l - y_m\right\} = \operatorname{sgn}\left\{1 - 2\frac{I_1}{I_1+I_2}\right\} \tag{20}$$

where $m,l \in \{1,2,3\}$ and

$$\operatorname{sgn}\{x\} = \begin{cases} -1, & x<0 \\ 0, & x=0 \\ +1, & x>0 \end{cases}$$

In particular, if $\operatorname{sgn}\left\{\frac{k_m}{k_l}y_l - y_m\right\} = 0$ it follows that $I_1/(I_1+I_2) = I_2/(I_1+I_2) = 1/2$. In this case, we can solve for *d* from the magnitude squared (see Eq. (15)) to obtain

$$d = \frac{1}{k_l}\cos^{-1}\left(2\left|\mu(k_l)\right|^2 - 1\right) \tag{21}$$

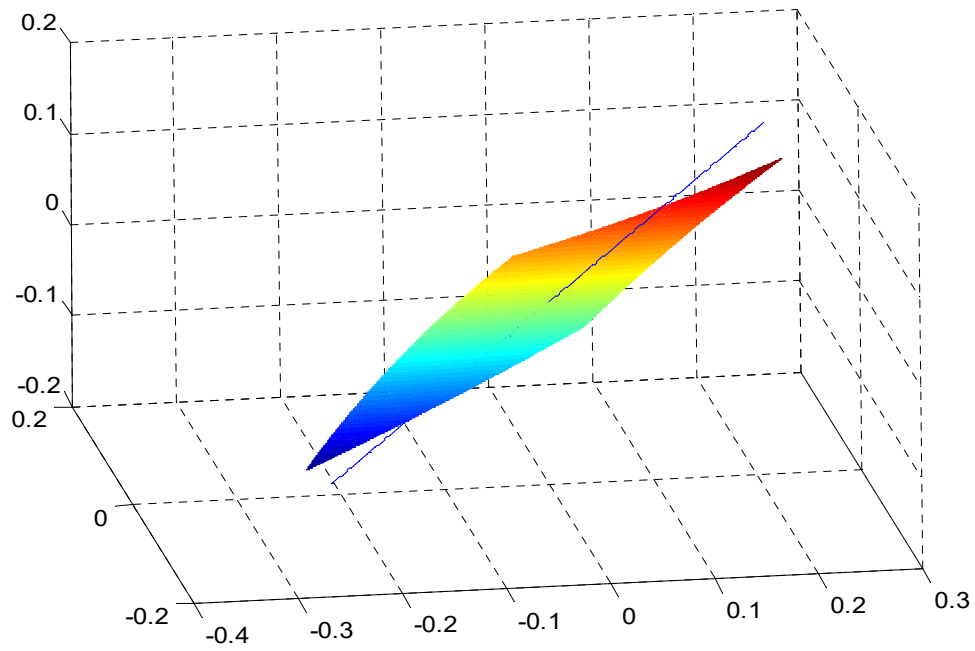

(a)

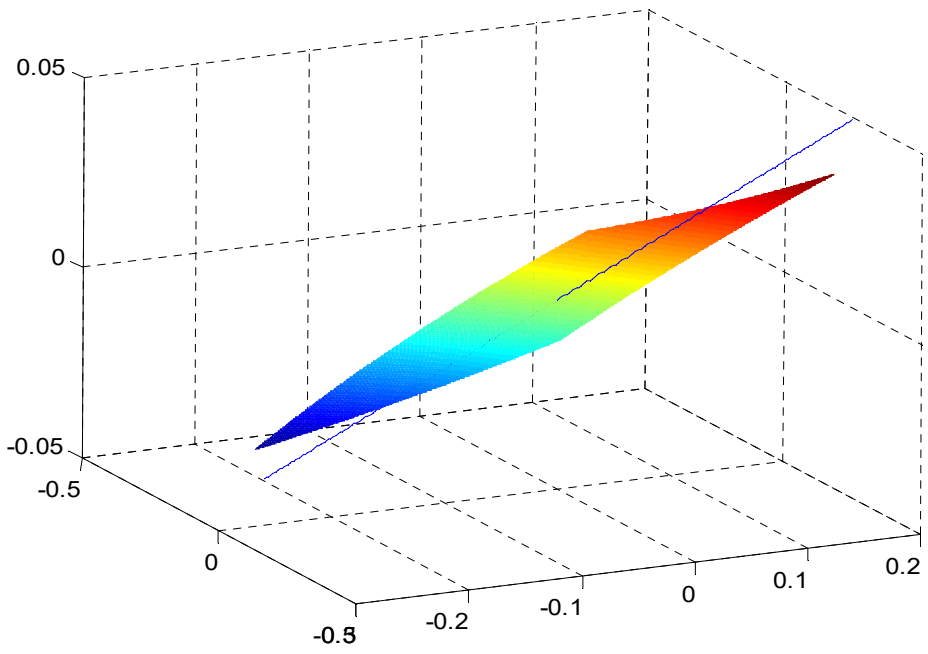

(b)

Figure 25. In both figures $d=\left(\sin\theta_2-\sin\theta_1\right)/2\approx 1$ **and** $s=\left(\sin\theta_1+\sin\theta_2\right)/2=0$. **In (a)** $k_1=1$, $k_2=0.55$, **and** $k_3=0.45$. **In (b)** $k_1=1$, $k_2=0.8$, **and** $k_3=0.2$.

where $\left|\mu(k_l)\right|$ is a measured quantity. Since $t_l(1/2, d) = 0$, the sum s is given by:

$$s = \frac{1}{k_l} y_l \tag{22}$$

We turn now to the case $I_1/(I_1 + I_2) \neq I_2/(I_1 + I_2)$.

Let us assume that $\operatorname{sgn}\left\{\frac{k_m}{k_l} y_l - y_m\right\} > 0$ so that $1 - 2I_1/(I_1 + I_2) > 0$ or $0 < I_1/(I_1 + I_2) < 1/2$. The case $\operatorname{sgn}\{(k_m/k_l) y_l - y_m\} < 0$ is similar. We introduce the surface S defined by (see Figure 25a and Figure 25b)

$$S = \left\{\mathbf{Z}(\alpha, \beta) \;\middle|\; 0 < \alpha < 1/2\,,\, 0 < \beta < \pi/(2k_l)\right\} \tag{23}$$

where

$$\mathbf{Z}(\alpha, \beta) = \left(y_1 - t_1(\alpha, \beta)\,,\, y_2 - t_2(\alpha, \beta)\,,\, y_3 - t_3(\alpha, \beta)\right) \tag{24}$$

and $t_l(\alpha, \beta)$ is defined by Eq. (16). (Since, by assumption $0 < I_1/(I_1 + I_2) < 1/2$, we need only consider values for α between 0 and 1/2. Also, we assume that the difference d satisfies the inequalities $0 < d < \pi/(2k_1)$, so that we only need to consider values for β between 0 and $0 < d < \pi/(2k_1)$.) The unknown parameters can be determined from the unique intersection of the surface S with the line L defined by

$$L = \left\{\mathbf{r}(\eta) \;\middle|\; |\eta| < b\right\} \tag{25}$$

where

$$\mathbf{r}(\eta) = (k_1\eta, k_2\eta, k_3\eta) \tag{26}$$

and b is an upper bound for $|s|$. At the intersection of S and L, we have

$$k_l\eta = y_l - t_l(\alpha, \beta), \text{ for } l = 1, 2, 3 \tag{27}$$

Let us denote by $\hat{\alpha}$, $\hat{\beta}$, and $\hat{\eta}$ the values of α, β, and η, respectively, at the intersection. Since the intersection is unique (see [33]), it follows that

$$I_1/(I_1 + I_2) = \hat{\alpha} \tag{28}$$

$$d = \hat{\beta} \tag{29}$$

and

$$s = \hat{\eta} \tag{30}$$

as desired. The figures (Figure 25a and Figure 25b) display the surface *S*, the line *L*, and their intersection for two different choices of the parameters: k_1, k_2, and k_3.

To provide for a more computationally efficient method of searching for the intersection, it may be advantageous to represent the surface in standard form. For this, we choose a coordinate system that enables us to represent *S* in the form

$$S = \left\{ \left(z_1, z_2, g\left(z_1, z_2 \right) \right) \;\middle|\; \left(z_1, z_2 \right) \in D \right\} \tag{31}$$

for some domain *D* and function $g\left(z_1, z_2 \right)$. This is possible because the Jacobian matrix of $\mathbf{Z}$ has rank two (see [32]); in fact, every pair of rows in the Jacobian matrix has non-zero determinant, so we may use the coordinate system defined, at least locally, by

$$z_l = y_l - t_l\left(\alpha, \beta \right), \qquad l = 1, 2\,. \tag{32}$$

The functions $\alpha\left(z_1, z_2 \right)$ and $\beta\left(z_1, z_2 \right)$, defined implicitly by Eq. (32), satisfy

$$\alpha\left(z_1, z_2 \right) = \frac{1}{2}\left[1 - \frac{\tan\left(y_2 - z_2 \right)}{\tan\left(k_2 \beta \right)} \right] = \frac{1}{2}\left[1 - \frac{\tan\left(y_1 - z_1 \right)}{\tan\left(k_1 \beta \right)} \right] \tag{33}$$

and

$$G\left(z_1, z_2, \beta \right) \equiv \frac{\tan\left(k_2 \beta \right)}{\tan\left(k_1 \beta \right)} - \frac{\tan\left(y_2 - z_2 \right)}{\tan\left(y_1 - z_1 \right)} = 0 \tag{34}$$

for the domain $D = \left\{ \left(z_1, z_2 \right) : 0 < y_l - z_l < \pi/2, l = 1, 2, \; \textit{and} \;\; \tan\left(y_2 - z_2 \right) / \tan\left(y_1 - z_1 \right) < k_2 / k_1 \right\}$.

(Here, the function $G\left(z_1, z_2, \beta \right)$, used to define β, is obtained by rearranging the last two expressions in Eq. (33).) The function $\beta\left(z_1, z_2 \right)$ is defined implicitly by Eq. (34), and, in turn, is used to define $\alpha\left(z_1, z_2 \right)$ via Eq. (33). We note that $G\left(z_1, z_2, \beta \right)$ is a strictly decreasing function of β with $G \to k_2 / k_1$, as $\beta \downarrow 0$ and $G \to 0$ as $\beta \uparrow \pi / \left(2 k_1 \right)$. It follows that $\beta\left(z_1, z_2 \right)$ is defined for every ordered pair $\left(z_1, z_2 \right)$ in the domain *D*. It can be shown that the function

$$\mathbf{u}\left(z_1, z_2 \right) = \left(\alpha\left(z_1, z_2 \right), \beta\left(z_1, z_2 \right) \right) \tag{35}$$

is one-to-one on the domain *D*. In this coordinate system, we have

$$z_l = y_l - t_l \circ \mathbf{u}(z_1, z_2), \quad l = 1,2, \tag{36}$$

and the function $g(z_1, z_2)$ is given by

$$g(z_1, z_2) = y_3 - t_3 \circ \mathbf{u}(z_1, z_2), \tag{37}$$

By inserting the map **u** into Eq. (24), we obtain

$$\mathbf{Z} \circ \mathbf{u}(z_1, z_2) = (z_1, z_2, g(z_1, z_2)) \tag{38}$$

We have produced the standard representation for the surface *S*.

We note that it is not necessary to compute the (z_1, z_2)-coordinate system. We may plot the surface *S* using the definition of $\mathbf{Z}(\alpha, \beta)$ given by Eq. (24) and then find the point $\mathbf{Z}(\alpha, \beta)$ that is closest to the line *L*. We have introduced the coordinate transformation as a means of providing for an alternative approach to finding the intersection. Also, this change of variables gives us an explicitly defined method for representing *S* in standard form.

The figures show the intersection of *S* and *L* for the case when the separation between the two targets is approximately two thirds the distance required by the Rayleigh criterion. In Fig. 25a, the smaller baselines are nearly equal; $k_1 = 1$, $k_2 = 0.55$, and $k_3 = 0.45$. In Fig. 25b, the smallest baseline is one fifth the length of the longest baseline; $k_1 = 1$, $k_2 = 0.8$, and $k_3 = 0.2$. In either case, the intersection is clearly discernable; however, the difference in the "slopes" at the intersection is greater for the case involving the longer baselines. This agrees with the intuitive conjecture which asserts that the longer baselines are less sensitive to noise. The validity of this conjecture is evident in this experiment as well as in several of the experiments presented in this report.

The advent of noise in the system causes a translation in the surface and, in turn, produces a shift in the location of the intersection. This effect may be studied using the model developed for this method. Additional study may provide methods that would enable us to optimize the design parameters of a multi-phase-center IFSAR. In addition to providing a practical method for resolving the layover problem, this method may prove to be a useful tool for analyzing the limit to the resolving power of the system in the presence of noise.

DISCUSSION OF RESULTS

Although there are only a few simulations and they are for only the subspace estimation techniques, we will use these to make some general conjectures. The first conjecture is that the general trends that are observed for the MUSIC technique are likely true for the ML method. For example, increasing the SNR of the targets allows us to resolve targets that are closer together. This is true for ML, as well as MUSIC, methods. The main difference between the ML and MUSIC method is that, where convergence can be achieved, the ML method will outperform the MUSIC method in lower SNR environments. The trends between the two are similar.

Another trend that is observed is that increasing either the small or largest baseline improves performance. Increasing the SNR and baseline length follows from our intuition from the traditional IFSAR case. There are a couple of new insights for the two-target case. One is that the farther apart the targets are in angle (e.g., farther apart in height), the better the performance. Another is that performance of estimating both targets improves as their amplitudes become similar. The reader should note the words "both targets" as being the key in the last sentence. The reason for this is that as one target gets brighter than the other, the results tend back toward the traditional IFSAR for the single target case. We have already seen that the single target case performs better than the two-target case.

A final note on this section is about what we mean by the word "performance". In this case we are meaning the bias and spread of the estimates of the spatial frequencies of the two targets. Recall that we have assumed that we are trying to estimate parameters of the sinusoids. These parameters are the frequency and the amplitudes of these sinusoids. We want to know how well the algorithms perform in estimating these parameters. Since we are operating below the Rayleigh resolution criteria, these algorithms are sometimes lumped in with the "super-resolution" techniques. In the case of parametric techniques, the "resolution" is a measure of the spread of the estimate of the frequency parameter. We see from the simulation results that the higher the spread in the distribution of the spatial frequency estimate (height, in the plots), the more difficult it is to distinguish, let alone estimate the frequencies of, two closely spaced targets.

One thing that has not been emphasized in this report is the errors associated with choosing the wrong model for parametric estimates. We have briefly touched upon these in the section on extended targets. Maybe more subtle was the discussion throughout this report on the errors made by traditional IFSAR when it assumes a model of a single target when in fact there are two targets present. It is obvious from this last example that using parametric techniques is important for their success.

It was noted that the two-target method did not perform as well as traditional IFSAR for a single target. One way to improve this is to add more phase centers. The problem with this is that it is expensive to add more phase centers and more radar channels. It is likely that ML methods and the direct method will provide some additional improvement, as well.

PRACTICAL CONSIDERATIONS

A list of practical considerations and other ideas are presented in the section, in no particular order.

1. We do not need to estimate multiple targets except where indicated by the "model order" process. This will save greatly on processing.
2. We could fly by twice with a two-antenna IFSAR and use techniques described in [34].
3. Three phase-centers do not provide enough degrees-of-freedom to estimate layover within a single range-Doppler bin. However, ambiguities can be resolved throughout the image with three phase centers, as long as there is not an ambiguity within the bin with two targets.
4. In practice, using ML may not be as complicated, because traditional IFSAR gives us a starting point and searching past an ambiguity is unnecessary because we cannot resolve an ambiguity within a range-Doppler bin anyway with only 3 antennas.
5. Estimating only two targets for complicated targets, such as trees and layover in hills is likely an improvement over assuming one target in traditional IFSAR, but this requires additional study.
6. The van Cittert-Zernike theorem says that there is height information within the magnitude of the correlation. It seems like it would be noisy, but perhaps adjacent information around the building could be used in conjunction with the magnitude of the correlation to solve building layover in another manner.

POSSIBLE FUTURE WORK

Since this was a mid-year LDRD, the time and funding did not permit us to investigate everything we would like to have for this topic. In fact, it felt like we were just getting momentum at the time the LDRD ended. (This topic was proposed for a full LDRD; however, the full LDRD did not receive funding.) Some of those additional investigations are listed below.

1. It would be highly desirable to apply this to real data sets. We recognized from the outset that this would be difficult to do on midyear LDRD funding, so it was not included only as desirable, and not as a requirement for this LDRD. In addition, available data sets for this purpose are quite limited.
2. Further simulation and testing of the direct method are appropriate and desirable.
3. Examine throughput performance improvements for all algorithms considered in this report.
4. Investigations of other spectral estimation techniques, such as Capon's algorithm, RELAX, array interpolation, and some of the wideband algorithms, as they apply to IFSAR could be valuable.
5. Intriguing properties of the amplitude estimation were noted in the simulations, but not presented in this report. It would be interesting to further examine these properties.
6. Investigation of the performance of the two target algorithms for the more complicated layover structures of trees and sloped terrain.
7. Extension of the algorithms to more phase centers and more targets.
8. Investigate the tie-in of these methods with true 3D imaging in sparse target environments.
9. Development of design algorithms for choosing appropriate system designs, e.g., baseline lengths, etc. for multiple baseline systems. Also, development of tools for estimating performance given a particular system and baseline lengths, etc.
10. Further investigate the performance of the proposed model order selection method.
11. Do a more extensive comparison of these methods with traditional endoclutter GMTI methods and STAP to better understand the relationship between the two and understand where applications of each method make sense.
12. Investigate combining MUSIC and ML approaches.
13. Finally, I mention again the need to apply it to real data, because it is important. That is where the rubber meets the road.

CONCLUSIONS

We have presented a couple of methods, including the development of a unique new method for estimating two targets with three or more phase centers. A simulation was developed for emulating IFSAR for two targets, such as buildings. The simulation results are presented for one of the methods. We also briefly compared the multiple phase center problem in IFSAR with the multiple phase center problem in GMTI, and found that the multiple phase center problem

These techniques show promise for resolving important two target problems, such as building layover. They certainly provide great improvement when two targets are present, over the traditional IFSAR, which assumes that there is only a single target present. They will likely provide improvement for more complicated targets, such as trees and sloped terrain, as well. It is probably unreasonable to assume that multiple targets can be resolved as well as a single target without the expense of many phase centers. It is possible to obtain the multiple phase centers at the cost of multiple passes by the target.

We ignored the very important and difficult task of calibrating and maintaining calibration of multiple phase center systems. This task should in no means be underestimated, particularly in costing a new system, and in the development and maintenance of multiple systems.

“Well, I can't put it any more clearly, sir, for it isn't clear to me.”

-- Alice in Disney's version of "Alice in Wonderland"

REFERENCES

[1] FGAN-FHR/EL AER-II: an airborne experimental radar, http://www.fhr.fgan.de/fhr/el/el_facil_aer00_e.html

[2] B. L. Burns, P. H. Eichel, W. H. Hensley, T. J. Kim, "IFSAR for the Rapid Terrain Visualization Demonstration," *Conference Record of the Thirty-Fourth Asilomar Conference on Signals, Systems and Computers*, 2000.

[3] D. Petit, F. Adrangna, J. D. Durou, "The filtering of layover areas in high resolution IFSAR for building extraction," *Proceedings of the EOS/SPIE Symposium on Remote Sensing*, Barcelona, Spain, Sept. 25-29, 2000.

[4] G. Burkhart, Z. Bergen, R. Carande, J. R. Fellerhoff, W.H. Hensley, D. L. Bickel, "Elevation Correction and Building Extraction from Interferometric SAR Imagery," *Proceedings of IGARSS'96*, 1996, pp. 659-661.

[5] P. Gamba, B. Housmand, "Three dimensional urban characterization by IFSAR measurements," *IEEE Trans. on Geoscience and Remote Sensing*, Vol. 1, 1999, pp. 302-304.

[6] A. Reigber, A. Moreira, "First Demonstration of Airborne SAR Tomography Using Multibaseline L-Band Data," *IEEE Trans of Geoscience and Remote Sensing*, Vol. 38, No. 5, Sept. 2000, pp. 2142-2152.

[7] D. L. Bickel, W. H. Hensley, D. A. Yocky, "The effect of scattering from buildings on interferometric SAR measurements," *Proceedings of IGSARSS'97*, 1997, pp. 1545-1547.

[8] D. L. Bickel, "A null steering viewpoint of interferometric SAR," *Proceedings of IGARSS'00*, 2000.

[9] F. Lombardini, F. Gini, P. Matteucci, "Application of Array Processing Techniques to Multibaseline InSAR for Layover Solution," *Proceedings of the 2001 IEEE Radar Conference*, Atlanta, GA, 2001.

[10] S. M. Kay, *Modern Spectral Estimation – Theory and Practice*, Prentice-Hall, 1988.

[11] I. Ziskind, M. Wax, "Maximum Likelihood Localization of Multiple Sources by Alternating Projection," *IEEE Trans. on Acoustics, Speech, and Signal Processing*, Vol. 36, No. 10, Oct. 1988, pp. 1553-1560.

[12] P. Stoica, R. Moses, *Spectral Analysis of Signals*, Prentice-Hall. 2005.

[13] J. Tsao, B. D. Steinberg, "Reduction of Sidelobe and Speckle Artifacts in Microwave Imaging: The CLEAN Technique," *IEEE Trans. on Antennas and Propagation*, Vol. 35, No. 4, April, 1988, pp. 543-556.

[14] J. Li and P. Stoica, "Efficient Mixed-Spectrum Estimation with Applications to Target Feature Extraction," *IEEE Trans on Signal Processing*, Vol. 44, No. 2, Feb. 1996, pp. 281-295

[15] T. B. Vu and H. Chen, "Real-time null steering by the CLEAN technique," *Int. J. Electronics*, Vol. 83, No. 4, 1997, pp. 541-553.

[16] F. Lombardini, P. Montanari, F. Gini, "Reflectivitiy Estimation for Multibaseline Interferometric Radar Imaging of Layover Extended Sources," *IEEE Trans on Signal Proc.*, Vol. 51, No. 6, June 2003, pp. 1508-1519

[17] F. Lombardini, J. Ender, L. Ro*f*Àing, M. Galletoo, L. Verranzzani., "Experiments of Interferometric Layover Solution with the Three-antenna Airborne AER-II SAR System," *Proc. of IGARSS 2004*, Sept. 2004, pp. 3341-3344

[18] R. O. Schmidt, *A Signal Subspace Approach to Multiple Emitter Location and Spectral Estimation*, PhD Thesis, Stanford University, 1982.

[19] R. Roy, T. Kailath, "ESPRIT – Estimation of Signal Parameters Via Rotational Invariance Techniques," *IEEE Trans. on Acoustics, Speech, and Signal Processing*, Vol. 37, No. 7, July 1989, pp. 984-995.

[20] D. L. Bickel, J. M. Delaurentis, Memo to L. M. Wells titled "Relationship between MUSIC and IFSAR", dated April 25, 2005.

[21] S. Haykin, *Adaptive Filter Theory, 2nd Ed.*, Prentice-Hall, 1991.

[22] V. F. Pisarenko, "The retrieval of harmonics by linear prediction," *Geophys J. R. Astron. Soc.*, vol. 33, pp. 347–366, 1973.

[23] A.J. Barabell, "Improving the resolution performance of eigenstructure based direction-finding algorithms," in *Proc. ICASSP'83*, pp. 336-339, Boston, MA, 1983.

[24] A. Manikas, *Differential Geometry in Array Processing*, Imperial College Press, 2004.

[25] G. Strang, K. Borre, *Linear Algebra, Geodesy, and GPS*, Wellesley-Cambridge Press, 1997.

[26] B. Friedlander, "The root-MUSIC algorithm for direction finding with interpolated arrays," *Signal Processing*, Vol. 30, pp. 15-29.

[27] C. V. Jakowatz, D. E. Wahl, P. H. Eichel, D. C. Ghiglia, P. A. Thompson, *Spotlight-Mode Synthetic Aperture Radar: A Signal Processing Approach*, Kluwer Academic Publishers, 1996.

[28] C. V. Jakowatz, D. E. Wahl, "Three-dimensional tomographic imaging for foliage penetration using multiple-pass spotlight-mode SAR", *Proceedings of the 35th Asilomar Conf. Signal, Systems, and Computers*, 2001.

[29] G. Fornaro, F. Lombardini, F. Serafino, "First Experiments of Adaptive 3D SAR Tomography with Repeat-Pass Spaceborne Data," *Proceedings of the 5th European Conference on Synthetic Aperture Radar*, May 25-27, 2004, Ulm, Germany, pp. 329-332.

[30] M. Zatman, "How narrow is narrowband," *IEE Proc. Radar Sonar Navig.* 145 (2) (April 1998) 85-91.

[31] D. A. Yocky, "Interferometric Coherence Classification Utility Assessment", *Proceedings of IGARSS'98*, Jul., 1998, pp. 1784-1786.

[32] E. Kreyszig, *Differential Geometry*, Dover, 1991.

[33] John M. DeLaurentis, Douglas L. Bickel, *Multi-Phase-Center IFSAR*, Sandia National Laboratories Report SAND2005-8018, Unlimited Release, January 2006.

[34] A. Martinez, A. W. Doerry, M. Jamshidi, D.L. Bickel, "Coherent Data Alignment and Baseline Calibration for Improved Two-Pass Interferometric SAR," SPIE Optical Engineering Journal, Vol. 42, No. 8, Aug. 2003, pp. 2427-2438.

APPENDIX: MAXIMUM LIKELIHOOD ESTIMATOR FOR SINUSOIDS IN GAUSSIAN NOISES

Assume that we have

K = number of elements in the array

N_s = number of distinct target locations (sinusoids)

N_L = number of samples or "snapshots"

Assume that we receive a return signal of the following form:

$$X = A(\Theta)S + N \tag{39}$$

where

$A(\Theta)$ = the array manifold matrix (array response to targets at angle Θ, sometimes referred to as steering vector), K by N_s matrix

S = the signal emitted by targets, N_s by N_L matrix

N = the noise matrix, K by N_L matrix

X = the output matrix from the array, K by N_L matrix

The joint probability density function (PDF) is given as in [11]:

$$f(X) = \prod_{i=1}^{N_L} \frac{1}{\pi \det\left[\sigma^2 I\right]} \exp\left(-\frac{1}{\sigma^2} \left| x_i - A(\Theta) s_i \right|^2 \right) \tag{40}$$

where

x_i = i^{th} column in X (which has N_L columns)

s_i = i^{th} column in S (which has N_L columns)

det[ ] is the determinant

Throwing away the constant, the log-likelihood function becomes:

$$L = -N_L K \log \sigma^2 - \frac{1}{\sigma^2} \sum_{i=1}^{N_L} \left| x_i - A(\Theta) s_i \right|^2 \tag{41}$$

Maximizing with respect to σ^2 leads to:

$$\frac{dL}{d\sigma^2} = 0 = -\frac{N_L K}{\sigma^2} + \left(\frac{1}{\sigma^2}\right)^2 \sum_{i=1}^{N_L} \left| x_i - A(\Theta) s_i \right|^2 \tag{42}$$

$$\hat{\sigma}^2 = \frac{1}{N_L K} \sum_{i=1}^{N_L} \left| x_i - A(\Theta) s_i \right|^2 \tag{43}$$

where:

$\hat{\sigma}^2$ = the maximized σ^2

Substituting back in and again throwing out constants, the ML estimator becomes:

$$\max_{\Theta,S} \left\{ -N_L K \log \left(\frac{1}{N_L K} \sum_{i=1}^{N_L} \left| x_i - A(\Theta) s_i \right|^2 \right) \right\} \tag{44}$$

or equivalently:

$$\min_{\Theta,S} \left\{ \sum_{i=1}^{N_L} \left| x_i - A(\Theta) s_i \right|^2 \right\} \tag{45}$$

As pointed out in [11], the above derivation has just shown that the ML estimator for sinusoids in Gaussian noise reduces to the least-squares problem given in Eq. (45).

The next step follows from [10, 11] is to minimize the amplitude (s_i) assuming that we know the spatial frequencies of the target locations (Θ). Taking the derivative and setting it to zero leads to:

$$A^H \left(x_i - A s_i \right) = 0 \tag{46}$$

leading to the solution:

$$\hat{s}_i = \left(A^H A \right)^{-1} A^H x_i \tag{47}$$

Plugging back into Eq. (45) yields:

$$\min_{\Theta} \left\{ \sum_{i=1}^{N_L} \left| x_i - A(\Theta) \left(A^H(\Theta) A(\Theta) \right)^{-1} A^H(\Theta) x_i \right|^2 \right\} \tag{48}$$

The following is readily recognizable as the projection matrix [25]:

$$P_A = A(\Theta)\left(A^H(\Theta)A(\Theta)\right)^{-1}A^H(\Theta) \tag{49}$$

The projection matrix, P_A, is the matrix that projects the data vector, x_i onto the subspace of the matrix containing the array steering vectors, $A(\Theta)$. Now Eq. (48) becomes:

$$\min_{\Theta}\left\{\sum_{i=1}^{N_L}\left|x_i - P_A x_i\right|^2\right\} = \min_{\Theta}\left\{\sum_{i=1}^{N_L}\left(x_i - P_A x_i\right)^H\left(x_i - P_A x_i\right)\right\} = \min_{\Theta}\left\{\sum_{i=1}^{N_L}\left(x_i^H x_i - x_i^H P_A^H P_A x_i\right)\right\} \tag{50}$$

We can observe that maximizing the projection minimizes Eq. (50) as follows:

$$L(\Theta) = \sum_{i=1}^{N_L}\left|P_A x_i\right|^2 \tag{51}$$

where

$L(\Theta)$ = the likelihood ratio quantity we want to maximize with respect to Θ

A final interesting form can be obtained when we define the sample covariance matrix as:

$$R = \frac{1}{N_L}\sum_{i=1}^{N_L} x_i x_i^H \tag{52}$$

Eq. (52) can be combined with Eq. (51) to give:

$$L(\Theta) = \mathrm{tr}\{P_A R\} \tag{53}$$

where

tr{ } = the trace operator.

Distribution

Unlimited Release

Email—Internal

all members	534x	
Technical Library	9536	libref@sandia.gov

Sandia National Laboratories is a multimission laboratory managed and operated by National Technology & Engineering Solutions of Sandia LLC, a wholly owned subsidiary of Honeywell International Inc. for the U.S. Department of Energy's National Nuclear Security Administration under contract DE-NA0003525.